

Polyhedral Surfaces of Constant Mean Curvature

Konrad Polthier

Feb. 17, 2002

Contents

Preface	vii
1 Introduction to Polyhedral Meshes	1
1.1 Simplicial Complexes	2
1.2 Topological Properties	6
1.3 Distance and Metric	8
1.4 Discrete Gauß Curvature	9
1.5 Grids in Numerics and Graphics	15
1.5.1 Delaunay Triangulation	18
1.5.2 Voronoi Diagrams	20
1.5.3 α -Shapes	21
1.6 Finite Element Spaces	22
1.6.1 Non-Conforming Finite Elements	23
2 Discrete Geodesics on Polyhedral Surfaces	25
2.1 Review of Smooth Geodesics	27
2.2 Discrete Straightest Geodesics	29
2.3 Discrete Geodesic Curvature	34
2.4 Parallel Translation of Vectors	37

2.4.1	Geodesic Runge Kutta	39
2.5	Geodesic Flow	42
2.5.1	Circles on Surfaces and the Geodesic Flow	44
2.5.2	Computing Discrete Distance Circles	47
2.5.3	Dynamic Computation of a Wave Texture	48
3	Conjugation of Discrete Harmonic Maps	51
3.1	Review of Smooth Harmonic Maps	53
3.2	Discrete Dirichlet Energy	54
3.3	Non-Conforming Harmonic Maps	60
3.4	Conjugate Harmonic Maps	63
3.5	Minimizing with Conjugate Gradients	69
3.6	Discrete Laplace Operators	72
3.7	Extension to Bezier Polyomials	75
4	Discrete Minimal Surfaces	79
4.1	Review of the Smooth Variation of Area	80
4.2	First Variation of the Discrete Area and Volume	81
4.3	Discrete Mean Curvature	83
4.4	Properties of Discrete Minimal Surfaces	88
4.5	Computing Discrete Minimal Surfaces	90
4.6	Conjugate Pairs of Discrete Minimal Surfaces	94
4.6.1	Discrete Conjugate Minimal Surface	97
4.6.2	Numerical Conjugation	100
4.7	Discrete Minimal Catenoid	101
4.8	Discrete Minimal Helicoid	109
5	Discrete Constant Mean Curvature Surfaces	113
5.1	Complete Discrete Examples	115
5.2	Prerequisites	118
5.3	Discrete Minimal Surfaces in \mathbb{S}^3	121
5.4	Discrete CMC Surfaces via Conjugation	128
5.5	Conjugate Surface Construction in \mathbb{S}^3	132
5.6	Solving Period Problems	135
6	Second Variation of Discrete CMC Surfaces	139
6.1	Non-Uniqueness of Discrete Minimal Disks	140
6.2	Jacobi Operator for Smooth CMC Surfaces	143

6.3	Second Variation of Area	147
6.4	Jacobi Operator for Discrete CMC Surfaces	151
6.5	Approximating Smooth Spectra	153
7	Singularities of Discrete Vector Fields	159
7.1	Setup	162
7.2	Discrete Rotation	163
7.3	Discrete Divergence	166
7.4	Hodge Decomposition of Vector Fields	171
7.5	Detecting Vector Field Singularities	174
7.5.1	Decomposition Algorithm	174
7.5.2	Examples	177
8	Interpolation of Adaptive Triangulations	183
8.1	Bisection Method of Rivara	184
8.2	Triangle Hierarchy	187
8.3	Interpolating Different Hierarchies	190
8.4	Applications	195
	References	201

1

Introduction to Polyhedral Meshes

Polyhedral meshes belong to the most basic structures for the representation of geometric shapes not only in numerics and computer graphics. Especially the finiteness of the set of vertices and of their combinatorial relation makes them an ideal tool to reduce infinite dimensional problems to finite problems. In this section we will review the basic combinatorial and topological definitions and state some of their differential geometric properties.

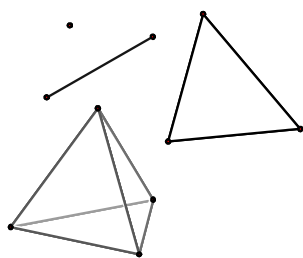
In practice, a variety of different triangle and other polyhedral meshes are used. In this introduction we restrict ourselves to simplicial complexes, or conforming meshes, where two polygons must either be disjoint or have a common vertex or a common edge. Or for short, a polygon is not allowed to contain a vertex of another polygon in the interior of one of its edges. This restriction avoids discontinuity problems in the shape, so-called hanging nodes. Further, we restrict our discussion to piecewise linear meshes although many concepts extend to meshes with piecewise higher order polynomial order. Often it is too restrictive to work solely in the space of conforming triangulations, and, in later chapters, we will enlarge the function space to include discontinuous, non-conforming meshes as well.

In many situations a property of a polyhedral surface can be associated to depend either on the geometric shape or on the combinatorial respectively topological properties of the mesh. Therefore, it

is important to distinguish between the topology of a mesh and its geometric shape which is determined by the geometric position of the vertices. For example, assume that all points of a compact surface are collapsed to a single geometric position, then we would still like to derive the topological genus from the combinatorial properties of the surface. This forces us to introduce slightly more abstract definitions of polyhedral surfaces.

Introductions to polyhedral manifolds are given in most books on algebraic topology, for example by Munkres [81], in the book by Ziegler [120] on combinatorial aspects of polytopes, or by Bloch [12] on topological and differential geometric problems. But note, there are slight differences depending on the purpose. The standard approach in topology introduces simplices and simplicial complexes as embeddings into Euclidean space while we allow immersions with self-intersections. Good sources of applications of polyhedral manifolds to problems in differential geometry are also the books by A.D. Alexandrov and Zalgaller [1] and Reshetnyak [103].

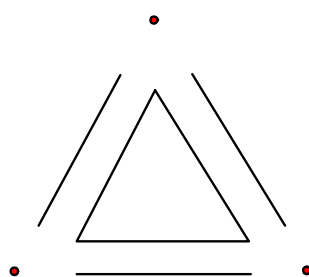
1.1 Simplicial Complexes



Low dimensional simplices.

We begin the introduction of polyhedral surfaces with a combinatorial point of view, that means, for the moment we do not care about the specific nature of points but consider them as abstract entities. In the combinatorial setup the most basic entities of polyhedral shapes are points, line segments, triangles, tetrahedrons, and their higher dimensional analogues, called simplices:

Definition 1 Let $\mathfrak{V} = \{v_0, \dots, v_m\}$ be a finite set of $m + 1$ abstract points. The (unordered) set $[v_0, \dots, v_m]$ is called a combinatorial m -simplex, or short, a combinatorial simplex. The number m is called the dimension of the simplex.



Faces of a triangle.

Definition 2 A face f of a simplex $\sigma = [v_0, \dots, v_m]$ is a simplex determined by a non-empty subset of $\{v_0, \dots, v_m\}$. A k -face has $k + 1$ points. A proper face is any face different from σ .

For example, a 0-simplex is a combinatorial point, a 1-simplex is a line segment, a 2-simplex is a triangle, and a 3-simplex is a tetrahedron. There exist seven faces of a triangle $[v_0, v_1, v_2]$: the triangle itself $[v_0, v_1, v_2]$, its three edges $[v_0, v_1]$, $[v_1, v_2]$, $[v_2, v_0]$ and its three points $[v_0]$, $[v_1]$, $[v_2]$, where the last six faces are proper. A 0-simplex has no proper face.

To perform the transition from combinatorics to geometry, we use the so-called standard simplex which serves as geometric representative associated to each combinatorial simplex:

Definition 3 The standard simplex $\Delta^m \subset \mathbb{R}^{m+1}$ is the convex hull of the endpoints $\{e_0, \dots, e_m\}$ of the unit basis vectors in \mathbb{R}^m which are given by $e_i = (0, \dots, 0, 1, 0, \dots, 0)$. Formally,

$$\Delta^m = \left\{ \sum_{i=0}^m \lambda_i e_i \mid 0 \leq \lambda_i \leq 1, \sum_{i=0}^m \lambda_i = 1 \right\}.$$

Note, the standard simplex not only is a set of points but includes the "interior" points. For example, the standard triangle Δ^2 in \mathbb{R}^3 is the planar triangle spanned by the three points $(1, 0, 0)$, $(0, 1, 0)$, $(0, 0, 1)$. Nevertheless, the standard simplex is simply a technical term. It provides the ground to formulate that any set of $m + 1$ points in a Euclidean space \mathbb{R}^n defines a geometric simplex:

Definition 4 A geometric simplex $\sigma = [p_0, \dots, p_m]$ is a set $V = \{p_0, \dots, p_m\}$ of $m + 1$ points in \mathbb{R}^n , where n might be different from m , together with an affine map

$$\begin{aligned} \varphi : \Delta^m &\rightarrow \text{convHull}(p_0, \dots, p_m) \\ \varphi(e_i) &= p_i. \end{aligned}$$

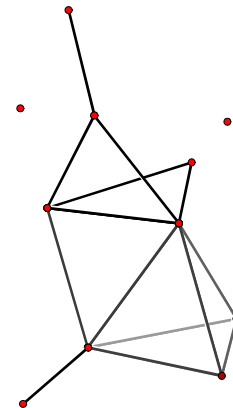
The number m is called the dimension of the simplex.

The difference between an abstract and a geometric simplex is the existence of the geometric realization provided by the map φ , that means, the embedding of the simplex in a vector space.

Definition 5 Let $\mathfrak{V} = \{v_1, v_2, \dots\}$ be a set of abstract points. Then an abstract simplicial complex K is a set of simplices S formed by finite subsets of \mathfrak{V} such that if $\sigma \in S$ is a simplex, then every subset $\tau \subset \sigma$ is also a simplex of K .

If two, or more, simplices of K share a common face, they are called adjacent or neighbours. The boundary of K is formed by any proper face that belongs to only one simplex, and its faces.

The simplicial complex K formally represents the connectivity of a mesh, and its simplices represent the points, edges, triangles, and higher dimensional simplices. The number of points in a complex may be infinite. By associating the set of abstract points with geometric



Simplicial Complex.

points in some \mathbb{R}^n we obtain a geometric shape consisting of piecewise flat simplices. Note, the following definition does not require an embedding but allows that the geometric realization may have self-intersections. By allowing immersions this definition is non-standard in the sense of algebraic topology which usually requires embeddings.

Definition 6 A simplicial complex (K, V) of an abstract simplicial complex K is a geometric realization uniquely given by

1. a set of geometric points $V = \{p_1, p_2, \dots\} \subset \mathbb{R}^n$ with a bijection

$$\Phi : \mathfrak{V} \rightarrow V$$

$$v_i \rightarrow p_i.$$

2. for each k -simplex $\sigma = [p_{i_0}, \dots, p_{i_k}]$ an affine map from the standard simplex

$$\varphi : \Delta^k \rightarrow \text{convHull}(p_{i_0}, \dots, p_{i_k})$$

$$\varphi(e_j) = p_{i_j}.$$

The above definitions ensure a strict separation between the combinatorial properties of a mesh specified by K and its geometric shape determined by V , which is also expressed by adding V to the notation of the simplicial complex (K, V) . The identification of abstract and geometric vertices is uniquely performed by the bijection Φ which relates the abstract points \mathfrak{V} of K and the set of geometric points V . Any embedding of the abstract complex K into a Euclidean space induces a topology on the simplicial complex.

Definition 7 The underlying (topological) space $|K|$ of a simplicial complex K immersed into \mathbb{R}^n is the topological space consisting of the subset of \mathbb{R}^n that is the union of all geometric realizations of simplices in K with the topology induced from any embedding of K .

Important examples of simplicial complexes are simplicial disks and balls.

Definition 8 A simplicial n -ball B^n is a simply connected simplicial complex such that $|B^n|$ is homeomorphic to the solid unit ball in \mathbb{R}^n , and a simplicial n -sphere S^n is homeomorphic to the boundary sphere of the solid unit ball in \mathbb{R}^{n+1} . For $n = 2$, B^2 is also called a simplicial disk, and S^2 is a simplicial sphere. For $n = 1$, S^1 is a simplicial circle.

For example, an icosahedron is a simplicial sphere, and any simply closed polygon is a simplicial circle.

In some cases it makes sense to identify a simplicial complex (K, V) with its underlying set $|K|$ in a Euclidean space \mathbb{R}^n , for example, a polytope can always be recovered from its set of vertices. In the general case one should keep in mind that (K, V) has more the character of an immersion. For example, if the immersion of a polygonal circle intersects geometrically at a point shaping a figure-eight then it may still be a combinatorial respectively topological circle. Note that the topology of such a shape cannot be recovered solely from its shape.

Definition 9 Let (K, V) be a simplicial complex. Then a subset $L \subset K$ is a subcomplex of K if L is a simplicial complex itself. For example, let $\sigma \in K$ be a simplex, then

$$\text{star } \sigma := \{\eta \in K \text{ that contains } \sigma, \text{ and all faces of } \eta\}$$

and

$$\text{link } \sigma := \{\eta \in \text{star } \sigma \mid \eta \cap \sigma = \emptyset\}.$$

are subcomplexes of K .

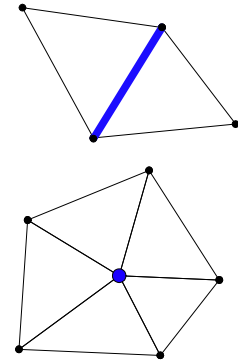
Simplicial surfaces extend the notion of a topological 2-manifold to the simplicial world.

Definition 10 A simplicial surface S is a simplicial complex consisting of a finite set \mathfrak{T} of triangles such that

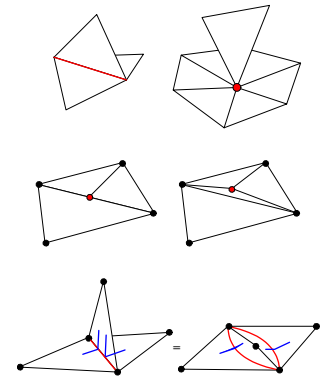
1. Any point $p \in S$ lies in at least one triangle $T \in \mathfrak{T}$.
2. The star of each point $p \in S$ is a simplicial disk.

Note, in the definition one may allow a denumerable set of triangles under the additionally assumption that the simplicial complex is locally finite, that is, the star of each vertex consists of a finite number of triangles.

A *polyhedral surface* is more general than a simplicial surface and may include flat faces with more than three vertices. The margin figure illustrates several pitfalls and degenerate situations which arise in practical implementations. The first row shows two non-manifold situations. The second row is a hanging node where adjacent faces do not join a common edge. The third row shows a valid simplicial surface consisting of four triangles where the pairwise adjacency of triangle pairs is indicated by two small lines. The right figure is a sketch to show how the middle edge belongs to all four triangles.



Star of an edge and a vertex.



Degenerate situations and non-manifold surfaces.

Care must be taken to avoid the first two situations in practical implementations. The third situation can be resolved with an additional neighbourhood information.

Definition 11 Let $M \subset \mathbb{R}^n$ be a topological surface. Then a simplicial surface S triangulates M if there exists a homeomorphism

$$t : |S| \rightarrow M.$$

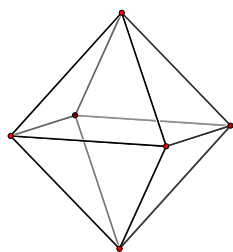
The simplicial complex S together with the homeomorphism t is called a triangulation of M .

Smooth surfaces and simplicial surfaces are related through the following theorem, compare [78]:

Theorem 12 The following facts hold for two-dimensional surfaces:

(1) Any compact topological surface M in \mathbb{R}^n can be triangulated, i.e. there exists a simplicial surface which triangulates M .

(2) If a topological surface is triangulated by two simplicial surfaces K_1 and K_2 , then K_1 and K_2 have simplicially isomorphic subdivisions.

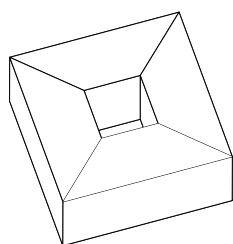


Octahedron

Often it is useful to enumerate the highest-dimensional simplices of a complex in a special way.

Definition 13 A shelling of a simplicial ball B^n is a listing of its n -simplices $\{\sigma_1, \dots, \sigma_m\}$ such that for all $1 \leq k \leq m$ the subset $\{\sigma_1, \dots, \sigma_k\}$ is a simplicial ball.

Any simplicial disk is shellable [78], but this result does not hold in higher dimensions. For example, see [107] for an unshellable subdivision of a tetrahedron.



Cube with hole.

1.2 Topological Properties

Euler Characteristic and Genus

Certain properties of a polyhedral surface S do not depend on the combinatorial triangulation but are already determined by the topological properties of $|S|$. For example, let v denote the number of points, e the number of edges and f the number of faces of S . Then the Euler characteristic $\chi(S)$ is defined by

$$\chi(S) = v - e + f \quad (1.1)$$

For example, $\chi(\text{Octahedron}) = 2$ or $\chi(\text{Cube with a hole}) = 0$. This counting procedure extends to higher dimensional simplicial complexes.

Definition 14 Let K be a simplicial complex, and let $f_i(K)$ denote the number of i -simplices of K . Then the Euler-Poincaré characteristic is defined as

$$\chi(K) = \sum_{i \geq 0} (-1)^i f_i(K).$$

Note, that these concepts do not require a simplicial complex but extend to polyhedral complexes.

The Euler characteristic is a topological invariant. In higher dimensions the proof involves machinery from algebraic topology but for surfaces the invariance is easily shown: Let M be a compact topological surface with two different triangulations (K_1, t_1) and (K_2, t_2) . Then we know that K_1 and K_2 have simplicially isomorphic subdivisions, and therefore have equal Euler number. But note, the inverse of this theorem is not true: if the Euler characteristics of two simplicial complexes K_1 and K_2 are the same then $|K_1|$ and $|K_2|$ need not be homeomorphic.

Therefore one speaks of the Euler characteristic of a compact 2-dimensional manifold M , which may be determined by an arbitrary triangulation \mathfrak{T} of M . For example, $\chi(\text{Sphere}) = 2$, $\chi(\text{Torus}) = 0$ or $\chi(\text{Projective Plane}) = 1$.

Orientable surfaces without boundary may be classified by the genus, a different topological invariant. Simply speaking, a surface M with genus $g(M)$ is topologically equivalent, i.e. homeomorphic, to a sphere with g handles attached. For orientable surfaces the Euler characteristic and the genus are equivalent invariants with the relation

$$2 - 2g(M) = \chi(M). \quad (1.2)$$

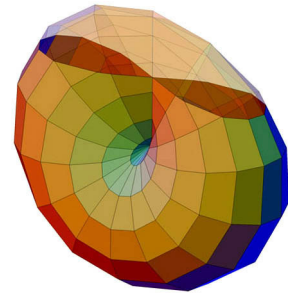
If M is a triangulation without boundary then, counting multiplicities, each face contributes three edges and each edge belongs to two face which leads to

$$3f = 2e.$$

Therefore, on simplicial surfaces with many triangles

$$\chi(M) = v - \frac{f}{2} = v - \frac{1}{3}e$$

7



The cross cap is a realization of the projective plane.

we have roughly about two times more faces than vertices, and three times more edges than vertices.

Triangulations with Boundary

Many practical applications use triangulations with a boundary where each component is a simply connected closed polygon. The Euler characteristic helps to verify the combinatorics of triangulations in this context too. Let b be the number of boundary components of a triangulation, and assume all boundaries are pairwise disjoint, i.e. they have no vertex in common. Then the Euler characteristic $\chi(M)$ is defined as above and is a topological invariant of the manifold with boundary, i.e. M is homeomorphic to a compact surface with Euler characteristic $\chi(M) + b$ from which b discs are removed. In this case we associate to M the genus of its closed companion.

Let us note simple examples which can be used to verify the correctness of a triangulation:

1. Let M be a planar bounded triangulation with b boundary components. Then we have

$$2 - \chi(M) = b \tag{1.3}$$

since M can be closed to a sphere with $\chi(S^2) = 2$ by pasting with b simply connected faces.

2. In general, an oriented polyhedral surface M with genus g and with b missing disks has b boundary components and fulfills

$$2 - 2g - \chi(M) = b. \tag{1.4}$$

Note, that both identities provide an easy way to calculate the number of boundary components if the genus is known, or to validate a given mesh if the genus and the number of boundaries are known.

1.3 Distance and Metric

For metric measurements the interior of simplicial faces must be uniquely defined. Therefore, we prefer simplicial instead of polyhedral surfaces, or assure that we work with piecewise flat polygons. The metric of a surface may, for example, be induced from an immersion into a Euclidean space, or the metric may be defined in a more

abstract way, say, by assigning a length to each edge which fulfills the triangle identity on each triangle. In a locally Euclidean metric the distance between two points is measured along curves whose length is measured segment-wise on the open edges and triangles:

Definition 15 *A curve γ on a simplicial complex M is called rectifiable, if for every simplex $\sigma \in M$ the part $\gamma|_{\sigma}$ is rectifiable w.r.t. to the smooth metric of σ . Then the length of γ is given by*

$$L(\gamma) := \sum_{\sigma \in M} L(\gamma|_{\sigma}). \quad (1.5)$$

as the sum of the lengths on each open simplex.

The area of a simplicial surface is defined in a similar way:

Definition 16 *Let M be a simplicial surface. Then we define*

$$\text{area } M := \sum_{T \in M} \text{area } M|_T. \quad (1.6)$$

Most of our considerations apply to a more general class of length spaces. Each face may have an arbitrary metric as long as the metrics of two adjacent faces are compatible, i.e. if the common edge has the same metric in both faces, and the triangle inequality holds.

In many practical applications simplicial complexes have a metric induced from an immersion into a Euclidean \mathbb{R}^n . For example, take a polyhedral surface in \mathbb{R}^3 and consider the two adjacent faces of an edge. Each face has the metric induced from \mathbb{R}^3 , i.e. the length of any curve on a face is equal to the length of the same curve measured in \mathbb{R}^3 . In this case, any neighbourhood of a point on the edge is isometric to a planar domain, since both faces can be unfolded to \mathbb{R}^2 .

When considering the approximation of a smooth surface M with a sequence of polyhedral surfaces $\{M_{h,i}\}$ one should be aware that higher order terms such as area may not converge as expected. The *Schwarz example* is a sequence of polyhedral surfaces which converges uniformly to a cylinder while the corresponding area grows to infinity.

1.4 Discrete Gauß Curvature

For a smooth surface S embedded into \mathbb{R}^3 the curvature measures the infinitesimal bending of the surface compared to the flat tangent

plane. Instead of comparing the surface with the tangent plane, we can equally consider the turn of the normal vector along the surface. Formally, this is measured by the *Gauß map* $g : S \rightarrow \mathbb{S}^2$ which assigns to each point p on a surface S the tip of its normal vector $n(p)$ after it was parallel translated to the origin of \mathbb{R}^3 , see Figure 1.1. The *total Gauß curvature* $K(\Omega)$ of a domain $\Omega \subset S$ is then given by the area of its spherical image including multiplicities: $K(\Omega) = \text{area } g(\Omega)$. The *Gauß curvature* $K(p)$ at a point p on S is defined as the limiting value

$$K(p) = \lim_{\varepsilon \rightarrow 0} \frac{\text{area } g(U_\varepsilon(p))}{\text{area } U_\varepsilon(p)} \quad (1.7)$$

for open neighbourhoods $U_\varepsilon(p)$ of radius less than ε of p . Note, if the surface S is twice differentiable, then the Gauß curvature can be expressed in terms of the partial derivatives of the metric tensor of S or as product $K(p) = \kappa_1(p)\kappa_2(p)$ of the two principal curvatures at p .

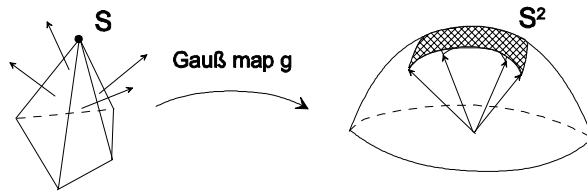


FIGURE 1.1. The Gauß map assigns to each point $p \in S$ of a surface its normal vector $n(p) \in \mathbb{S}^2$. At edges and vertices of a polyhedral surface the image of the Gauß map is the spherical convex hull of the normal vectors of adjacent faces.

The Gauß curvature of a general manifold is a central intrinsic property of the geometry and is fully determined by the Riemannian metric. It influences, for example, the parallel translation of tangent vectors along curves of the manifold.

On a polyhedral surface, the discrete Gauß curvature is concentrated at the isolated vertices since all other points on the surface have a neighbourhood isometric to a planar Euclidean domain with zero curvature. But at vertices the limit value in Equation 1.7 will not exist unless the surface is planar. Therefore it is more appropriate to work with the concept of total Gauß curvature in the polyhedral case.

On a polyhedral surface, the neighbourhood of a vertex is isometric to a cone. Before defining a discrete Gauß curvature we study simplicial

cones in more detail. Metrically, each cone is characterized by the total vertex angle:

Definition 17 Let S be a polyhedral surface and $p \in S$ a vertex. Let $\{f_1, \dots, f_m\}$ be the set of faces of star p , and let θ_i be the vertex angle of the face f_i at the vertex p , see Figure 1.2. Then the total vertex angle $\theta(p)$ is given by

$$\theta(p) = \sum_{i=1}^m \theta_i(p). \quad (1.8)$$

Interior points p of a face or of an open edge have a neighbourhood which is isometric to a planar Euclidean domain, and we define $\theta(p) = 2\pi$ in these cases.

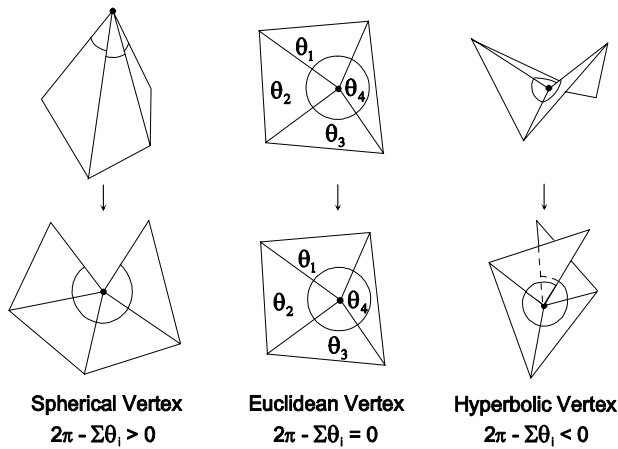


FIGURE 1.2. Classification of vertices on a polyhedral surface according to the excess of the vertex angle, and their unfolding to a planar domain.

All points of a polyhedral surface can be classified according to the sign of the *vertex angle excess* $2\pi - \theta(p)$:

Definition 18 A vertex p of a polyhedral surface S with total vertex angle $\theta(p)$ is called Euclidean, spherical, or hyperbolic if its angle excess $2\pi - \theta(p)$ is $= 0$, > 0 , or < 0 . Similarly, interior points of a face or of an open edge are always Euclidean.

The neighbourhood of a vertex can be isometrically unfolded to a (partial or multiple) covering of a part of the Euclidean plane. There

exist three situations as shown in Figure 1.2 which metrically characterize the vertex. For example, the tip of a convex cone is a spherical vertex and a saddle point is hyperbolic. On the other hand, a spherical vertex need not be the tip of a convex cone. The isometric unfolding of sets of a polyhedral surface is a common procedure to study the geometry.

The vertex angles determine the discrete Gauß curvature directly in metrical terms of the polyhedral surface S . For simplicity we restrict here to surfaces without boundary, compare Remark 21 for the Gauß curvature at boundary vertices.

Definition 19 *The discrete Gauß curvature $K(p)$ of an interior vertex p on a polyhedral surface S is defined as the vertex angle excess*

$$\begin{aligned} K(p) &= 2\pi - \theta(p) \\ &= 2\pi - \sum_{i=1}^m \theta_i(p). \end{aligned} \tag{1.9}$$

The total Gauß curvature $K(S)$ of the polyhedral surface S is the sum of the Gauß curvatures of all vertices of K

$$K(S) = \sum_{p \in K^{(0)}} K(p).$$

An immediate consequence is that Euclidean vertices have curvature $K = 0$, spherical vertices have $K > 0$, and hyperbolic vertices have $K < 0$. For example, the vertices of a cube each have Gauß curvature $\frac{\pi}{2}$.

As a justification of this first definition of a discrete curvature term, let us note the following remarkable consequence. The total Gauß curvature, above derived from the local geometric properties of the vertex stars, is related to the Euler characteristic and, therefore, has a global topological significance for the polyhedral surface.

Theorem 20 (Simplicial Gauß-Bonnet) *Let S be a compact polyhedral surface in \mathbb{R}^n without boundary. Then*

$$K(S) = 2\pi\chi(S).$$

Proof. First we triangulate S without affecting either side of the equation. Since S is compact without boundary we then have

$$3f = 2e$$

where v, e, f denotes the number of vertices, edges and faces of the surface S . Therefore we obtain

$$\begin{aligned}
\sum_{p \in K^{(0)}} K(p) &= \sum_{p \in K^{(0)}} (2\pi - \sum_{\sigma \in \text{star } p^{(2)}} \theta(p, \sigma)) \\
&= 2\pi v - \sum_{\sigma \in \text{star } p^{(2)}} \sum_{p \in K^{(0)}} \theta(p, \sigma) \\
&= 2\pi v - \pi f \\
&= 2\pi v - 2\pi e + 2\pi f \\
&= 2\pi \chi(S)
\end{aligned}$$

where $K^{(i)}$ denotes the i -dimensional simplices of a complex K . \square

Remark 21 *The Gauß curvature at boundary vertices of a bounded domain can be defined in different ways. [1] suggests to use the angle defect to π while we prefer to use the difference to the total vertex angle if the domain is part of a larger polyhedral surface. This view allows us to extend the theorem in Chapter 2 to bounded regions on surfaces by including the geodesic curvature of the simplicial boundary curve, see Theorem 4.3. We postpone this more general result until we have introduced the notion of discrete geodesic curvature of curves on polyhedral surfaces.*

Minimizing the Gauß Curvature

We consider the Plateau problem for the Gauß curvature which starts with a given boundary curve γ and looks for a disk or punctured higher genus patch spanned by γ which minimizes the Gauß curvature. By the smooth version of Gauß-Bonnet [24], the total Gauß curvature of any spanned patch M can be estimated from below by the total curvature of γ :

$$\int_M K da = 2\pi \chi(M) - \int_\gamma \kappa_g ds \geq 2\pi \chi(M) - \int_\gamma \kappa ds \quad (1.10)$$

since the geodesic curvature is always smaller than the curvature of a curve $0 \leq \kappa_g \leq \kappa$.

Therefore, in the smooth situation a curvature minimizing patch M can be immediately constructed:

1. create a small strip along γ which is tangent to the osculating plane and which has zero width along segments with vanishing curvature.

2. arbitrarily extend the strip to a patch with assumed genus.

The tangency condition ensures that within the strip the geodesic curvature of γ is pointwise equal to its curvature, and we obtain equality in Equation 1.10, i.e. M is curvature minimizing.

In the smooth case the ambiguity of the extension of the strip to the interior can be removed by looking for a curvature minimizing cone over the curve, at least up to some extent. Let p be the center of the cone connected with straight lines to γ . Assume $\gamma(t)$ is parametrized by arclength. Let $b := p - \gamma - \langle p - \gamma, \gamma' \rangle \gamma'$ be parallel to the co-normal vector along γ of the current cone, then the total geodesic curvature is given by

$$\int_0^\ell \kappa_g dt = \int_0^\ell \left\langle \gamma'', \frac{b}{|b|} \right\rangle dt.$$

It is maximized by variation of p in direction of the gradient

$$\frac{d}{dp} \int_0^\ell \kappa_g dt = \int_0^\ell \frac{1}{|b|} \left(\gamma'' - \left\langle \gamma'', \frac{b}{|b|} \right\rangle \frac{b}{|b|} \right) dt.$$

In the polyhedral case we start with a polygonal curve γ_h and given mesh connectivity, say by an initial surface $M_{h,0}$. Then it is generally not possible to find a strip with the combinatorics induced by $M_{h,0}$ such that γ_h has vanishing discrete normal curvature. But minimizing the Gauß curvature of the polyhedral surface will lead to a polyhedral immersion which approximates best the osculating plane along the boundary.

Let p be an interior vertex of the polyhedral surface and θ_i the vertex angle at p of a triangle Δ_i with edges $c_i = a_i - b_i$ and such that a_i, b_i emanate from p . Then the gradient of the vertex angle θ_i is given by

$$\begin{aligned} \nabla_p \theta_i &= \frac{\sin^2 \theta_i}{\text{area } \Delta_i} \left(\frac{a_i + b_i}{2} + \frac{1}{2} \cot \theta_i J c_i \right) \\ &= \frac{\sin^2 \theta_i}{\text{area } \Delta_i} (M_i - p) \end{aligned}$$

where M_i is the center of the circumcircle. Similarly, if q is a vertex adjacent to p , and θ the vertex angle at p then we have

$$\nabla_q \theta = \sum_{\Delta \in \text{star } pq} \frac{J_\Delta (p - q)}{|p - q|^2}$$

where J_Δ denotes the rotation by $\frac{\pi}{2}$ in the oriented plane of the triangle Δ . Summarizing, we obtain:

Lemma 22 *The gradient of the polyhedral Gauß curvature is given by*

$$\nabla_p K(p) = \sum_i \frac{\sin^2 \theta_i}{\text{area } \Delta_i} (p - M_i)$$

and

$$\nabla_q K(p) = \sum_{\Delta \in \text{star } pq} \frac{J_\Delta(q-p)}{|q-p|^2}.$$

where M_i is the center of the circumcircle.

These equations suffice to apply the conjugate gradient method for minimizing the Gauß curvature of M_h .

1.5 Grids in Numerics and Graphics

In recent years an enormous effort went into the design of efficient grids in numerics and computer graphics. Adaptive grids and hierarchical representations became very important in numerical applications, and are nowadays complemented with subdivision surfaces in computer graphics modeling packages. Among the current issues is the construction of specialized encodings for efficient data compression.

This section recalls some important types of meshes used in numerical computations and computer graphics. The choice of a suitable grid depends on a number of criteria such as the shape of the domain, the type of the numerical method, or even the hardware, for example, to support parallelization of algorithms.

Structured grids tessellate a rectangle $[x_{\min}, x_{\max}] \times [y_{\min}, y_{\max}] \subset \mathbb{R}^2$ into regular quadrilaterals of the same size $h = (h_x, h_y)$. The grid Ω_h

$$\Omega_h = \left\{ (x_i, y_j) \mid \begin{array}{l} x_i = x_{\min} + ih_x \quad i \in [0, m-1] \\ y_j = y_{\min} + jh_y \quad j \in [0, n-1] \end{array} \right\}$$

is implicitly determined by the two extremal vertices (x_{\min}, y_{\min}) and (x_{\max}, y_{\max}) and the number of subdivisions (m, n) . *Multiblock grids* use several structured grids at possibly different resolutions to cover the different regions of the domain. *Multigrids* and *sparse grids* are hierarchical representations which allow a considerable reduction of the number of grid points.

Parametric grids are obtained as images of other grid types under a continuous map Φ and thus are suitable for the discretization of more

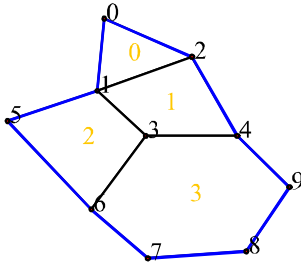
general domains. Important examples of parametric maps are Möbius maps and the Schwarz-Christoffel map, both are angle-preserving, i.e. conformal maps. Circle packings, remarkably applied by Thurston and others to problems with three-manifolds, are nowadays a promising concept in practical implementations, for example, for the flattening of rather general surfaces [63].

Unstructured or irregular grids may consist of rather general non-overlapping polygons. Such grids are determined by a set of points, i.e. the vertices of the polygons,

$$P = \{P_0, P_2, \dots, P_9\}$$

and connectivity information where each polygon is given as an ordered list of its vertices, or more efficient, of its vertex indices

$$\begin{aligned} E_0 &= \{0, 1, 2\} \\ E_1 &= \{2, 1, 3, 4\} \\ E_2 &= \{5, 6, 3, 1\} \\ E_3 &= \{3, 6, 7, 8, 9, 4\}. \end{aligned}$$



Unstructured Grid.

Additional information of a structured grid may be stored in order to achieve faster access of information, or to clarify ambiguous situations. For example, a list of neighbour faces which have common edge with the current face. The following neighbour array has for each element E_i a list of indices of adjacent elements N_i where $N_i[j]$ denotes the element adjacent to the edge $E_i[j+1]E_i[j+2]$ of E_i (indices are modulo number of vertices of E_i).

$$\begin{aligned} N_0 &= \{1, -1, -1\} \\ N_1 &= \{2, 3, -1, 0\} \\ N_2 &= \{3, 1, -1, -1\} \\ N_3 &= \{-1, -1, -1, -1, 1, 2\}. \end{aligned}$$

The naming convention has its origin in triangle meshes where the edge $E_i[j+1]E_i[j+2]$ is opposite to the vertex E_i . The above rule allows us to use the same programming code for both, simplicial as well as polyhedral surfaces.

In Chapter 8 we will introduce a hierarchical representation of irregular grids which allows a continuous interpolation between adaptively refined irregular meshes. This solves the interpolation problem in animations and for a set of adaptive geometries which depend on one or more parameters.

An alternative to vertex based formats are *facet-edges formats*. Here a set of edges is given as above by specifying pairs of vertex indices. Then higher dimensional cells are defined through their boundary, that means a two-dimensional element is determined by a set of edge indices. Such formats are useful if all cells of a cell-complex play an active role and have associated information.

The *winged edge format* was introduced by Baumgart [11] as a redundancy free representation format to store polyhedral meshes of faces with an arbitrary and varying number of edges. It is an edge-based format where each edge contains references to two vertices P_1 and P_2 , and references E_1 respectively E_2 to an adjacent edge on each of the two neighbouring faces. Boundary edges have one empty edge reference. It is assumed that each face has a unique orientation provided by an orientation of its edges. Therefore, faces are implicitly given by following the E_1 or E_2 reference of an arbitrary known edge of the face. Note, the orientation of each individual face does not require that the whole surface is oriented.

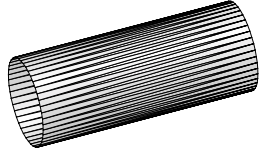
Compared to the unstructured grid representation introduced above the winged edge format basically requires the same amount of storage: let E be the number of edges and F be the number of faces. In the winged edge format each edge has four integer references which leads to a storage of size $4E$. By the relation $3F = 2E$ for triangular meshes, the amount $4E$ is equal to $6F$ for irregular meshes which store 3 vertex references and 3 links to adjacent faces per face.

Non-manifold meshes may have more than two faces sharing an edge. In this case both the winged-edge format as well as the surface mesh format fail unless additional information is supplied.

Progressive meshes introduced by Hoppe [60] are based on vertex-split and edge-collapse operations for adaptive refinement and coarsening. In recent years these data types have been very popular in computer graphics especially since they allow topology changes. They are a special class of *multi-resolution grids* or *hierarchical grids* which store different levels of resolution of a shape. Often a smooth transition between different hierarchical resolutions is incorporated in the data structure. *Normal meshes* [53] were designed to describe shapes locally as graph over a coarser resolution of the same mesh. This technique is especially suitable for *subdivision surfaces* or multi-resolution surfaces obtained from a wavelet decomposition where the finer resolutions are obtained algorithmically.

The fast and incremental transmission of shapes over low-bandwidth connections plays an increasing role nowadays. Here specialized representations of meshes allow a compressed encoding. For example, the

algorithm by Taubin and Rossignac [115], which is incorporated into the MPEG-4 standard, encodes the connectivity of a triangle mesh with about 2–3 bits per vertex compared to 96 bits used in the index based representation mentioned above.



Cylinder with thin triangles.

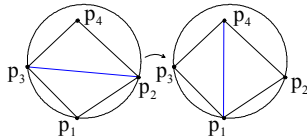
1.5.1 Delaunay Triangulation

In numerics and visualization long thin triangles are often avoided since their occurrence may spoil the numerical error and lead to artefacts in rendered images. This is mainly due to the fact that linear interpolation of values given at the vertices of such a triangle may not have a good approximation property in the center. Although in some cases long thin triangles are appropriate, like in the cylindrical shape in the figure, we make the following Definition.

Definition 23 Let P be the set of vertices of a triangulation T and $A(T) = (\alpha_1, \alpha_2, \dots)$, $\alpha_i \leq \alpha_j$ if $i < j$, the angle vector of all vertex angles in T . Then the triangulation T is called angle-optimal if for all triangulations T' the angle vector $A(T)$ is lexicographically larger than $A(T')$ ($A(T) > A(T')$), i.e. there exists an index i such that

$$\alpha_j = \alpha'_j \text{ for all } j < i, \text{ and } \alpha_i > \alpha'_i.$$

The lexicographic order of an angle vector of a triangulation can be increased by successive operations called *edge-flips*. This technique also avoids the computation of vertex angles.



Edge flip criterium.

Lemma 24 Consider two adjacent coplanar triangles with vertices p_1, p_2, p_3 and p_2, p_3, p_4 and common edge p_2, p_3 . If p_4 lies inside the circumcircle through p_1, p_2, p_3 then the angle-vector can be increased by exchanging edge p_2, p_3 with edge p_1, p_4 (edge flip). Furthermore, if the four points lie on a common circle, then both diagonal edges are fine.

Proof. Thales theorem allows to restrict the proof to a most symmetric situation from which the lemma follows by checking angles.

Let $a = (a_1, a_2)$ be the coordinates of four vertices of a planar, convex quadrilateral $\{a, b, c, d\}$, then it is easy to check that the edge bd must be flipped if and only if

$$\det \begin{pmatrix} a_1 & a_2 & a_1^2 + a_2^2 & 1 \\ b_1 & b_2 & b_1^2 + b_2^2 & 1 \\ c_1 & c_2 & c_1^2 + c_2^2 & 1 \\ d_1 & d_2 & d_1^2 + d_2^2 & 1 \end{pmatrix} > 0$$

□

For non-planar quadrilaterals in space a possible criterion is: the edge bd must be flipped if

$$\alpha + \delta > \beta + \gamma.$$

Definition 25 *A planar triangulation T of a point set P is Delaunay if the circumcircle of each triangle does not contain any point of P in its interior. This condition for being Delaunay is called the sphere test.*

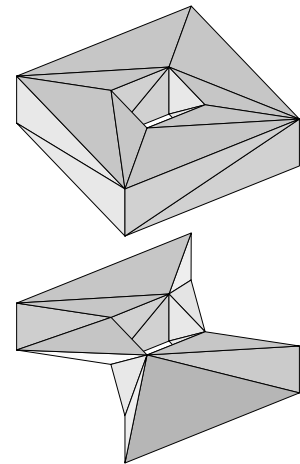
Obviously, any Delaunay triangulation is edge-optimal, and Lawson [71] showed that an edge-optimal triangulation is a Delaunay triangulation. Any angle-optimal triangulation is edge-optimal and therefore a Delaunay triangulation, and Delaunay triangulations are angle-optimal, if no four adjacent vertices of P lie on a circle. If four vertices of P lie on a circle then, at least, the Delaunay triangulation maximizes the minimum angle over all triangulations of P . Since any two triangulations of a planar point set can be transformed into each other [70], one can convert any initial triangulation to a Delaunay triangulation with the following edge swapping algorithm of Lawson [71]:

Algorithm 26 (Lawson 1977) *Let P be a given planar point set and a triangulation T' . Then the triangulation can be converted to a Delaunay triangulation T by a finite number of edge-flips, and T maximizes the minimal angle. Furthermore, if no four vertices of P lie on a common circle then T is angle-optimal.*

This algorithm is ensured to terminate since the number of possible angles in a triangulation is finite and in each edge flip the minimal angle is increased. We call such a triangulation edge-optimal. The algorithm is rather slow but stable and easy to implement.

Remark 27 *There should be some caution when using edge flips on non-planar surfaces in 3d space. On curved surfaces edge-flips may easily lead to degenerate situation even if care is taken on the valence of vertices. For example, the torus shown in the side figure is converted into a degenerate shape using a few edge-flips.*

If there is no initial triangulation of a point set P then there exist different algorithms for the direct construction of a Delaunay triangulation. For example, the algorithm of Watson [118] is based on inserting a point in an already existing Delaunay triangulation



A 3d geometry may degenerate through edge flips.

1. Construct a triangle which covers the convex hull of the given point set P . This single triangle is a simple Delaunay triangulation, and it will be removed later.
2. Insert a point of P in the existing triangulation and make the triangulation again Delaunay.
3. If all points of P have been inserted then remove the original triangle, otherwise continue with step 2.

The crucial work is done in step 2. If the new vertex lies inside a triangle then the triangle is split into three new triangles and the three old edges must be legalized. If the new vertex lies on an edge, then both triangles are bisected and the four old edges must be legalized. Of course, the legalization must be continued if edges are flipped. A further optimization considers sorting the point set P .

It is possible to build the Delaunay triangulation of a set of n points in \mathbb{R}^d in $O(n \log n + n^{\lceil \frac{d}{2} \rceil})$ expected time. The second term is the maximum number of possible simplices. In practice, the running time is much faster. A brute force algorithm starts with a simplex whose vertices are "at infinity", and adds a new vertex at each step while maintaining the Delaunay property through edge flips.

It should be noted that the Delaunay triangulation of a point set P contains interesting subgraphs, for example, the *minimum spanning tree* of P which connects all points of P with a set of edges of minimum total length.

1.5.2 Voronoi Diagrams

The Voronoi diagram of a set of points $P \subset \Omega \subset \mathbb{R}^d$ is a partitioning of Ω into cells where each cell c_i consists of the set of points $q \in \mathbb{R}^d$ which are closest to p_i . Finding a Voronoi diagram is often also called the Post Office Problem. A good introduction is the book by de Berg et al. [27] on computational geometry.

A promising strategy for tessellating the domain Ω with a given set of points P might associate to each point p a catchment area $V(p)$ of points closer to p than to any other point of P . For example, if P is the locations of good suppliers and Ω the region with people demanding goods, then for each supplier p the Voronoi region $V(p)$ is the area where people most efficiently go to location p for shopping. Formally,

Definition 28 If P is a point set in a domain Ω and $p \in P$. Then the Voronoi region $V(p) \subset \Omega$ is

$$V(p) = \left\{ r \in \Omega \mid d(p, r) = \min_{q \in P} d(q, r) \right\}.$$

The Voronoi diagram $V(P)$ consists of the boundaries of all Voronoi regions $V(p)$ with $p \in P$.

The boundaries of all Voronoi regions are the Voronoi graph of the Voronoi diagram. Each interior point on an edge of the Voronoi graph has the same distance to exactly two points p, q of P , and it is closer to p and q than to any other point in P . Each vertex v of the Voronoi graph is the center of the circumcircle of n points $p_1, p_2, p_3, \dots, p_n$ of P where n is the number of edges at v , respectively the number cells at v , and the circumcircle contains no point of P in its interior. If all vertices of the Voronoi graph have valence 3 then each triple (p_1, p_2, p_3) is a Delaunay triangle.

Theorem 29 Let $V(P)$ be the Voronoi diagram of a planar point set P and let $\{p_i, p_j, p_k\} \subset P$ represent three sites.

1. A point q is a vertex of $V(P)$ if and only if its largest empty circle $C(q)$ contains three or more points of P on its boundary.
2. The bisector between two sites p_i and p_j is an edge of the diagram if and only if there exists a point q on the bisector such that the circle $C(q)$ with center q through p_i and p_j contains no other point of P in its interior and on its boundary.

The best algorithms to compute the vertices of the Voronoi diagram of a set of n -sites P spend $O(n \log n)$ time.

The Delaunay graph of a point set P is a triangulation dual to the Voronoi diagram, and each edge of the Voronoi diagram is the mid-perpendicular of a Delaunay edge connecting both sites.

1.5.3 α -Shapes

α -shapes were introduced in the plane by Edelsbrunner et al. [39] in 1983 to provide a continuous transition from the set of vertices through a growing shape to the convex hull. The original definition was later extended to three-dimensional space [40]. Let P be a set of points and T its Delaunay triangulation. Each simplex $\sigma \in T$ is assigned a size $s(\sigma)$ which is the radius of the smallest sphere

enclosing σ . σ is called conflict-free if the smallest sphere does not contain any other point of P other than the vertices of σ .

Definition 30 The α -shape of a point set P with $\alpha \in \mathbb{R}_0^+$ is a sub-complex \sum_α of the Delaunay triangulation T consisting of all simplices $\sigma \in T$ with size $s(\sigma) < \alpha$ and which are conflict-free, as well as all their subsimplices.

The 0-shape consists of the set P of all vertices, and the ∞ -shape consists of the convex hull of P . If P is finite then the family of α -shapes is finite too.

1.6 Finite Element Spaces

Piecewise polynomial functions on simplicial surfaces conceptually fall into the category of finite element spaces. Here we briefly recall the most basic function spaces relevant for our later work. See the books [26][20] for an introduction.

Definition 31 On a simplicial surface M_h we define the function space S_h of conforming finite elements:

$$S_h := \{v : M_h \rightarrow \mathbb{R}^d \mid v \in C^0(M_h) \text{ and } v \text{ is linear on each triangle}\}$$

S_h is a finite dimensional space spanned by the Lagrange basis functions $\{\varphi_1, \dots, \varphi_n\}$ corresponding to the set of vertices $\{p_1, \dots, p_n\}$ of M_h , that is for each vertex p_i we have a function

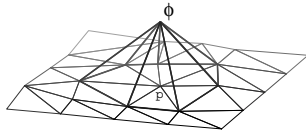
$$\begin{aligned} \varphi_i : M_h &\rightarrow \mathbb{R}, \varphi_i \in S_h \\ \varphi_i(p_j) &= \delta_{ij} \quad \forall i, j \in \{1, \dots, n\} \\ \varphi_i &\text{ is linear on each triangle.} \end{aligned} \tag{1.11}$$

Then each function $u_h \in S_h$ has a unique representation

$$u_h(p) = \sum_{j=1}^n u_j \varphi_j(p) \quad \forall p \in M_h$$

where $u_j = u_h(p_j) \in \mathbb{R}^d$. The function u_h is uniquely determined by its nodal vector $(u_1, \dots, u_n) \in \mathbb{R}^{dn}$.

Sometimes we will also use piecewise higher-order polynomial representations described in a similar way with different basis functions. Note that any component function of a function $v \in S_h$ has bounded Sobolev H^1 norm.



Basis function on manifold.

1.6.1 Non-Conforming Finite Elements

In our later investigations the following space of non-conforming finite elements, see [26][20] for a detailed discussion, plays an important role. Since these spaces include discontinuous functions their use is often titled as a *variational crime* in the finite element literature. In our settings, non-conforming functions naturally appear as the correct spaces for our later considerations on constant mean curvature surfaces.

Definition 32 For a simplicial surface M_h , we define the space of non-conforming finite elements by

$$S_h^* := \left\{ v : M_h \rightarrow \mathbb{R}^d \mid \begin{array}{l} v|_T \text{ is linear for each } T \in M_h, \text{ and} \\ v \text{ is continuous at all edge midpoints} \end{array} \right\}$$

The space S_h^* is no longer a finite dimensional subspace of $H^1(M_h)$ as in the case of conforming elements, but S_h^* is a superset of S_h . Let $\{m_i\}$ denote the set of edge midpoints of M_h , then for each edge midpoint m_i we have a basis function

$$\begin{aligned} \psi_i : M_h &\rightarrow \mathbb{R} & \psi_i &\in S_h^* \\ \psi_i(m_j) &= \delta_{ij} & \forall i, j &\in \{1, 2, \dots\} \\ \psi_i &\text{ is linear on each triangle.} \end{aligned} \quad (1.12)$$

The support of a function ψ_i consists of the (at most two) triangles adjacent to the edge e_i , and ψ_i is usually not continuous on M_h . Each function $v \in S_h^*$ has a representation

$$v_h(p) = \sum_{\text{edges } e_i} v_i \psi_i(p) \quad \forall p \in M_h$$

where $v_i = v_h(m_i)$ is the value of v_h at the edge midpoint m_i of e_i .

Let $M_h \subset \mathbb{R}^m$ be a conforming triangulation with vertices $V = \{p_1, p_2, \dots\}$ and edge midpoints $E = \{m_1, m_2, \dots\}$. For a given triangle $t \in M_h$ with vertices $\{p_{t_1}, p_{t_2}, p_{t_3}\}$ and edge midpoints $\{m_{t_1}, m_{t_2}, m_{t_3}\}$ we have the following elementary correspondence

$$\frac{1}{2} \begin{pmatrix} 0 & 1 & 1 \\ 1 & 0 & 1 \\ 1 & 1 & 0 \end{pmatrix} \begin{pmatrix} p_{t_1} \\ p_{t_2} \\ p_{t_3} \end{pmatrix} = \begin{pmatrix} m_{t_1} \\ m_{t_2} \\ m_{t_3} \end{pmatrix} \quad (1.13)$$

respectively

$$\begin{pmatrix} -1 & 1 & 1 \\ 1 & -1 & 1 \\ 1 & 1 & -1 \end{pmatrix} \begin{pmatrix} m_{t_1} \\ m_{t_2} \\ m_{t_3} \end{pmatrix} = \begin{pmatrix} p_{t_1} \\ p_{t_2} \\ p_{t_3} \end{pmatrix}. \quad (1.14)$$

We will also use the term *non-conforming surface* to denote a simplicial surface where adjacent triangles are connected at the midpoint of their common edge but may be twisted. Later we also require that the corresponding edge of two adjacent triangles must have the same length. Non-conforming surfaces may be considered as images of a non-conforming map from a conforming surface, therefore, we often do not distinguish between a non-conforming surface and a non-conforming map.

3

Conjugation of Discrete Harmonic Maps

Discrete harmonic maps appear as a basic model problem in finite element theory and differential geometry for the discretization of smooth concepts. Beyond that, discrete harmonic maps have a wide range of non-trivial applications in computer graphics, for example to smoothen noisy meshes, or in differential geometry to compute constant mean curvature surfaces.

Several discrete operators on simplicial surfaces are related to discrete harmonic maps. For example, the area gradient, the mean curvature, or the divergence operator on vector fields. The main topic of this section is the construction of pairs of conjugate discrete Laplace-Beltrami harmonic maps on polyhedral surfaces. We start to derive the definitions and properties of discrete harmonic maps in a geometric setting which will then allow us to develop other discrete geometric operators and to solve problems related to minimal and constant mean curvature surfaces in Chapters 4, 5 and 7.

Harmonic maps on surfaces also have practical importance, for example, we derive in Chapters 4 and 5 efficient numerical algorithms for solving free boundary value problems for unstable minimal surfaces and constant mean curvature surfaces. In the algorithms [87] and [85], the conjugate of a minimal surface is obtained via the conjugation of a discrete harmonic map. Conjugate harmonic maps are originally defined on the dual graph of the edge graph of the original

surface but one should consider them as non-conforming functions. The results of the present chapter provide a thorough understanding of the geometric constructions used in Pinkall and Polthier [87] and in Oberknapp and Polthier [85] by relating the discrete conjugation of surfaces to non-conforming finite element spaces.

Convergence of conforming harmonic maps has been shown by Tsuchiya [117]. As a more general result for surfaces, Dziuk and Hutchinson [36] obtained optimal convergence results in the H^1 norm for the finite element procedure of the Dirichlet problem of surfaces with prescribed mean curvature. Compare Müller et al. [80] for harmonic maps on planar lattices using the five-point Laplacian.

In a subsequent section we will apply the duality between discrete harmonic maps and their conjugates to define discrete conformal maps. We will extend a conformal energy proposed by Hutchinson [64] to the discrete spaces $S_h \times S_h^*$ and show that the discrete holomorphic maps have zero conformal energy, a property generically not available for conforming piecewise linear maps.

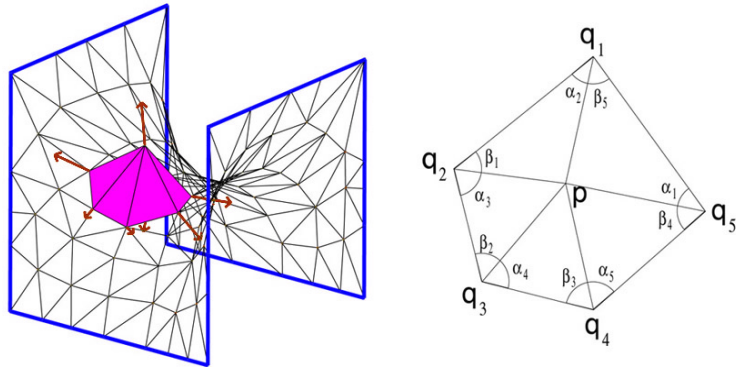


FIGURE 3.1. Discrete mean curvature vector on a polyhedral surface given as Laplace-Beltrami operator of the identity map from the surface to itself.

We start with a review of the Dirichlet problem of harmonic maps in Section 3.1 followed by the discretization using conforming Lagrange elements in Section 3.2. In Section 3.3 we discretize the same Dirichlet problem using the non-conforming Crouzeix-Raviart elements, and derive a pointwise expression of the discrete minimality condition. Section 3.4 contains the main results of this chapter, namely, identifying solutions in both finite element spaces as pairs of discrete conjugate harmonic maps. Applications of the results are given in Chapters

4 and 5 to the conjugation of discrete minimal and constant mean curvature surfaces.

3.1 Review of Smooth Harmonic Maps

On a Euclidean domain, the Laplace operator is given by the second partial derivatives

$$\Delta = \frac{\partial}{\partial x_1^2} + \dots + \frac{\partial}{\partial x_n^2}.$$

Harmonic maps $u : \Omega \rightarrow \mathbb{R}$ on an open set Ω in \mathbb{R}^n are solutions of the Laplace equation

$$\Delta u = 0 \text{ in } \Omega \tag{3.1}$$

which often appears with prescribed boundary conditions. Dirichlet conditions prescribe fixed boundary values in the form of a function g

$$u|_{\partial\Omega} = g \text{ on } \partial\Omega$$

and Neumann conditions prescribe the derivative of u in the direction of the normal ν of the boundary

$$\partial_\nu u|_{\partial\Omega} = \mu \text{ on } \partial\Omega.$$

Dirichlet and Neumann boundary conditions may appear simultaneously on disjoint segments of the boundary.

The Laplace operator of vector-valued maps, and thereby the harmonicity of vector-valued maps, is defined component-wise on each coordinate function. For functions $u : M \rightarrow \mathbb{R}$ on a manifold M with a Riemannian metric g the Laplace-Beltrami operator Δ_g is a generalization of the Laplace operator. Assume normal coordinates around a point p on M and let $\{e_1, \dots, e_n\}$ be the induced orthonormal frame in the tangent space of M , then

$$\Delta_g = \nabla_{e_1} \nabla_{e_1} + \dots + \nabla_{e_n} \nabla_{e_n}.$$

Harmonic maps also appear as minimizers of the *Dirichlet energy*

$$E_D(u) = \frac{1}{2} \int_M |\nabla u|^2 dx \tag{3.2}$$

with Dirichlet conditions (or Neumann) at the boundary, since the Laplace equation 3.1 is the Euler-Lagrange equation of the Dirichlet energy. To see this, let $u(t) := u_0 + t\phi : M \rightarrow \mathbb{R}$ be any C^1 -variation of

a function u_0 whose variation function has compact support $\phi|_{\partial M} = 0$. Then by differentiation and integration by parts we obtain

$$\begin{aligned} \frac{d}{dt}\Big|_{t=0} E_D(u(t)) &= \int_M \langle \nabla u, \nabla \phi \rangle \\ &= - \int_M \Delta u \cdot \phi + \int_{\partial M} \partial_\nu u \cdot \phi \end{aligned}$$

where ν is the exterior normal along ∂M . Since ϕ has compact support, the last integrand vanishes identically. Since the above equation holds for any C^1 -variation we derive

$$\nabla E_D(u) = 0 \iff \Delta u = 0$$

from the fundamental lemma of the calculus of variations. The minimizer u_{\min} is unique since

$$\begin{aligned} E_D(u_{\min} + \phi) &= E_D(u_{\min}) + E_D(\phi) \\ &> E_D(u_{\min}) \quad \forall \phi|_{\partial M} = 0, \phi \neq 0. \end{aligned}$$

where the cross term vanishes because of the minimality condition for u_{\min} .

3.2 Discrete Dirichlet Energy

There are different equivalent ways to introduce discrete harmonic maps. Here we use the characterization of harmonic maps as minimizers of the Dirichlet energy since this approach also provides an efficient numerical algorithm to solve the boundary value problems for discrete harmonic maps.

Definition 52 *Let M_h be a simplicial surface in \mathbb{R}^m and S_h the set of polyhedral maps on M_h . Then the Dirichlet energy of a function $u_h \in S_h$ with $u_h : M_h \rightarrow \mathbb{R}^d$ is given by*

$$E_D(u_h) := \frac{1}{2} \sum_{T \in \mathfrak{T}_h} \int_T |\nabla u_h|^2 dx. \quad (3.3)$$

That is, the Dirichlet energy of u_h is the sum of the Dirichlet energies of the smooth atomic maps $u_h|_T$ on each triangle T .

Now we consider critical points of the Dirichlet energy. For simplicity, we restrict to interior variations which keep the boundary values fixed.

Definition 53 A variation $\phi(t) \in S_h$, $t \in [0, \varepsilon)$, is a family of functions differentiable in t such that each map $u_h \in S_h$ gives rise to a family of maps $u_h(t) \in S_h$ with

$$u_h(t) = u_h + \phi(t)$$

Basically, a variation of a function $u_h \in S_h$ is a modification of its values at each vertex p_i of the triangulation M_h given by $u_h(t)(p_i) = u_h(p_i) + \phi(t)(p_i)$. For simplicity, we restrict to Dirichlet boundary conditions, that is, the variations $\phi(t)$ are zero along the boundary of M_h .

Definition 54 A critical point u_h in S_h of the Dirichlet energy (3.3) in S_h with respect to Dirichlet boundary conditions is called a discrete harmonic map.

In the following we derive an explicit representation of the Dirichlet energy of polyhedral maps and a system of equations for the discrete minimizers which characterize discrete harmonic maps.

Let $T = \{p_1, p_2, p_3\}$ be a triangle of a simplicial surface and oriented edges $\{c_1, c_2, c_3\}$ with $c_i = p_{i-1} - p_{i+1}$, and $\varphi_i : T \rightarrow \mathbb{R}$ be the Lagrange basis function at vertex p_i with $\varphi_i(p_j) = \delta_{ij}$. Then its gradient is

$$\nabla \varphi_i|_T = \frac{1}{2 \text{area } T} J c_i, \quad (3.4)$$

where J denotes rotation by $\frac{\pi}{2}$ oriented such that $J c_i$ points into the triangle. Note, that $\varphi_1 + \varphi_2 + \varphi_3 = 0$ implies $\nabla \varphi_i = -\nabla \varphi_{i-1} - \nabla \varphi_{i+1}$. The basis functions have mutual scalar products given by

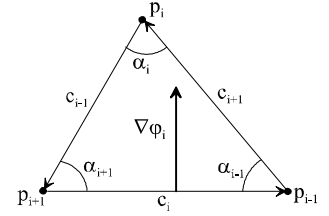
$$\begin{aligned} \langle \nabla \varphi_{i-1}, \nabla \varphi_{i+1} \rangle &= -\frac{\cot \alpha_i}{2 \text{area } T} \\ \langle J \nabla \varphi_i, \nabla \varphi_{i+1} \rangle &= \frac{1}{2 \text{area } T} \\ |\nabla \varphi_i|^2 &= \frac{\cot \alpha_{i-1} + \cot \alpha_{i+1}}{2 \text{area } T}. \end{aligned} \quad (3.5)$$

Since each function $u_h \in S_h$ has a representation

$$u_h(p) = \sum_{j=1}^n u_j \varphi_j(p) \quad p \in M_h,$$

where $u_j = u_h(p_j)$ denotes the function value of u_h at the vertex p_j of M_h , on a single triangle T the gradient of $u_h|_T : T \rightarrow \mathbb{R}^d$ is given by

$$\nabla u_h|_T = \frac{1}{2 \text{area } T} \sum_{j=1}^3 u_j J c_j. \quad (3.6)$$



Gradient of basis function.

Theorem 55 *Let M_h be a simplicial surface and S_h the set of continuous and piecewise linear functions on M_h . Then the discrete Dirichlet energy of any function $u_h \in S_h$ is given by*

$$E_D(u_h) = \frac{1}{4} \sum_{\text{edges } (x_i, x_j)} (\cot \alpha_{ij} + \cot \beta_{ij}) |u_h(p_i) - u_h(p_j)|^2. \quad (3.7)$$

Further, the minimizer of the Dirichlet functional (3.3) is unique and solves

$$\frac{d}{du_i} E_D(u_h) = \frac{1}{2} \sum_{x_j \in n(x_i)} (\cot \alpha_{ij} + \cot \beta_{ij}) (u_h(p_i) - u_h(p_j)) = 0 \quad (3.8)$$

at each interior vertex p_i of M_h . The first summation runs over all edges of the triangulation, and the second summation over all edges emanating from p_i . The angles α_{ij} and β_{ij} are vertex angles lying opposite to the edge (p_i, p_j) in the two triangles adjacent to (p_i, p_j) .

Proof. Using the explicit representation (3.4) of the basis functions and the identity $\nabla \varphi_i = -\nabla \varphi_{i-1} - \nabla \varphi_{i+1}$, we obtain the Dirichlet energy of $u_h|_T$:

$$\begin{aligned} E_D(u_h|_T) &= \frac{1}{2} \int_T - \sum_{j=1}^3 |u_{j+1} - u_{j-1}|^2 \langle \nabla \varphi_{j-1}, \nabla \varphi_{j+1} \rangle \\ &= \frac{1}{4} \sum_{j=1}^3 \cot \alpha_j |u_{j+1} - u_{j-1}|^2. \end{aligned}$$

Summation over all triangles of M_h and combining the two terms corresponding to the same edge leads to equation 3.7.

At each interior vertex p_i of M_h , the gradient of E_D with respect to variations of $u_i = u_h(p_i)$ in the image of u_h is obtained by partial differentiation and easily derived from

$$\frac{d}{du_i} E_D(u_h) = \int_{\Omega} \langle \nabla u_h, \nabla \varphi_i \rangle.$$

Since S_h is a finite dimensional space, the quadratic minimization problem for the Dirichlet energy has a unique solution u_h in S_h . \square

The definition of the Dirichlet energy of vector-valued maps $F_h : M_h \rightarrow N_h \subset \mathbb{R}^d$ is in full coherence with the definition of Dirichlet energy of scalar-valued maps. Namely, if the map $F_h = (f_1, \dots, f_d)$ has component functions $f_i : M_h \rightarrow \mathbb{R}$ then we have

$$E_D(F_h) = \sum_{i=1}^d E_D(f_i)$$

since $|\nabla F_h|^2 = |\nabla f_1|^2 + \dots + |\nabla f_d|^2$. Vector-valued harmonic maps are defined as critical values of the Dirichlet functional in the same way as in the scalar-valued case. Therefore, the balancing condition for scalar-valued harmonic maps directly gives a balancing formula for vector-valued discrete harmonic maps too.

The following definition includes more general boundary conditions. Neumann boundary conditions constrain the derivative of a function in direction of the exterior normal of the domain. Later we will make use of other boundary conditions which are useful for maps from a simplicial surface M_h to another surface N_h .

Definition 56 *A solution $u_h \in S_h$ of the Dirichlet problem (3.8) in S_h is called a discrete harmonic map. To include symmetry properties into this definition we allow in some cases also variation of boundary points:*

- *if a domain boundary arc and its corresponding image boundary arc are straight lines, then the interior boundary points may vary along the straight line in image space*
- *if both corresponding arcs are planar symmetry curves restricted to planes we allow variation of interior boundary points in the image plane. This models also free boundary value problems*
- *in all other cases the image boundary points remain fixed.*

Remark 57 *At each vertex x_i Equation (3.8) can be geometrically interpreted as a balancing condition for the weighted edges emanating from the vertex x_i . The weight of each edge solely depends on the angles in the base surface M_h , i.e. the weights depend only on the conformal structure of M_h .*

Examples of Discrete Harmonic Maps

Simple examples of discrete harmonic maps are derived from the observation that on the integer grid $\mathbb{Z} \times \mathbb{Z}$ in \mathbb{R}^2 the interpolants of some smooth harmonic functions are discrete harmonic:

Example 58 *On a rectangular $\mathbb{Z} \times \mathbb{Z}$ grid in \mathbb{R}^2 , which is triangulated by subdividing along either diagonal of each rectangle, the interpolating functions of*

$$\operatorname{Re} z, \operatorname{Re} z^2, \operatorname{Re} z^3, \text{ and } \operatorname{Im} z^4$$

are discrete harmonic maps, and so are the interpolants of some other polynomials.

Example 59 On a rectangular $\mathbb{Z} \times \mathbb{Z}$ grid in \mathbb{R}^2 , the weight of each diagonal is $\cot \frac{\pi}{2}$, and it vanishes independent of the chosen diagonal in each square. Therefore, at each grid point (i, j) only the discrete values of the five-point stencil

$$\{(i, j), (i, j - 1), (i - 1, j), (i + 1, j), (i, j + 1)\} \quad i, j \in \mathbb{Z}$$

of the finite difference Laplacian contribute to the Dirichlet gradient.

The next example leads to discrete harmonic maps on a simplicial surfaces using linear maps:

Definition 60 Let M_h be a polyhedral surface in \mathbb{R}^m . A map $u_h \in S_h(M_h)$ from M_h to \mathbb{R}^d is called a linear map if u_h is the restriction $u|_{M_h}$ of a linear map $u : \mathbb{R}^m \rightarrow \mathbb{R}^d$, i.e.

$$u_h = u|_{M_h} : M_h \rightarrow \mathbb{R}^d.$$

For example, any coordinate function $x_i : M_h \rightarrow \mathbb{R}$ on a polyhedral surface M_h is a linear map, and, more general, let $a \in \mathbb{R}^m$ be a constant vector, then

$$u_h(p) := \langle a, p \rangle \quad \forall p \in M_h$$

is linear.

On an arbitrary simplicial surface $M_h \subset \mathbb{R}^m$ the following geometric assumption on the underlying domain surface M_h leads to discrete harmonic functions:

Example 61 All linear maps $u_h : M_h \rightarrow \mathbb{R}^d$ on a polyhedral surface M_h are discrete harmonic if and only if M_h is a discrete minimal surface.

Proof. Using the Lagrange basis functions $\varphi_i : M_h \rightarrow \mathbb{R}$ associated to each vertex p_i of M_h we have the representation

$$u_h(x) = \sum_{p_i \in M_h} u_h(p_i) \varphi_i(p), \quad p \in M_h.$$

The gradient of the Dirichlet energy can be transformed using the linearity of u_h

$$\begin{aligned} \frac{d}{du_i} E_D(u_h) &= \frac{1}{2} \sum_{j \in n(i)} (\cot \alpha_{ij} + \cot \beta_{ij}) (u_h(p_i) - u_h(p_j)) \\ &= u_h \left(\frac{1}{2} \sum_{j \in n(i)} (\cot \alpha_{ij} + \cot \beta_{ij}) (p_i - p_j) \right) \\ &= u_h \left(\frac{d}{dp_i} E_D(\text{id}_h M_h) \right). \end{aligned}$$

Therefore, u_h is a critical value of the Dirichlet energy if and only if the identity map of M_h is discrete harmonic. The harmonicity of the identity map of a discrete minimal surface is shown in Corollary 92. \square

Mean Value Property and Maximum Principle

Among the two most important properties of smooth harmonic maps are the mean value property and the maximum principle.

Mean Value Property: Let $p \in M$ and $U_\varepsilon(p)$ be a disk with radius ε around p . Then the value of a smooth harmonic function u at the center p is the average of the values along the boundary of the disk

$$u(p) = \frac{1}{2\pi\varepsilon} \int_{|q-p|=\varepsilon} u(q).$$

We obtain a discrete version for polyhedral maps if we replace the disk with a regular polygon.

Lemma 62 *Let u_h be a discrete harmonic map defined on a simplicial surface M_h . If the star of a vertex p consists of congruent isosceles triangles centered at p then*

$$u_h(p) = \frac{1}{\#\text{link } p} \sum_{q_j \in \text{link } p} u_h(q_j)$$

is the center of mass of the function values $\{u_h(q_j)\}$ on the link of p .

Proof. All vertex angles appearing in Equation (3.8) are the same. \square

Maximum Principle: Since smooth harmonic maps solve an elliptic differential equation they satisfy a maximum principle. This means, in any open domain $U \subset M$ the maximum and minimum of u is attained

at the boundary ∂U . In the discrete case, a similar statement for the star of a vertex does not hold in general, for example, it may fail if the spatial domain contains angles larger than 90 degrees.

Lemma 63 *Let u_h be a discrete harmonic map defined on a spatial domain of a simplicial surface M_h formed by the points $\{q_j\}$ around a vertex p . If the triangles around p are all acute, then $u_h(p)$ is contained in the convex hull of the points $\{u_h(q_j)\}$.*

Proof. From the local harmonicity condition (3.8) we see that $u_h(p)$ can be represented as a linear combination of the points $\{u_h(q_j)\}$. Since all relevant angles are acute the weights of the $u_h(q_j)$ are in the interval $(0, 1)$, and $u_h(p)$ is a convex combination. \square

The two previous lemmas do not hold if we allow more general domains. For example, if the domain contains obtuse triangles as in the Example 4.4 then neither the mean value nor the convex hull property may be valid.

The non-convexity of discrete harmonic maps will lead to interesting counterexamples of the maximum principle of minimal surfaces in Chapter 4. In practical applications, for example, when smoothing meshes with a Laplace filtering or mapping surfaces onto a planar domain, then one would often like to ensure convexity. In these case the mesh parametrization by Floater [44] might be a useful strategy since it ensures convexity.

3.3 Non-Conforming Harmonic Maps

Non-conforming maps on simplicial surfaces were introduced in Section 1.6.1 as another natural set of discrete maps. Let M_h be a simplicial surface then we state the Dirichlet energy in the space S_h^* as in the previous section.

Definition 64 *Let M_h be a simplicial surface in \mathbb{R}^m . Then the Dirichlet energy of a function $v_h \in S_h^*$ with $v_h : M_h \rightarrow \mathbb{R}^d$ is given by*

$$E_D(v_h) := \frac{1}{2} \sum_{T \in M_h} \int_T |\nabla v_h|^2 dx.$$

That is, the Dirichlet energy of v_h is the sum of the Dirichlet energies of the smooth atomic maps $v_h|_T$ on each triangle T .

Now we consider critical points of the Dirichlet energy, and again, for simplicity, we restrict to interior variations which keep the boundary values fixed.

Definition 65 A variation $\Psi(t) \in S_h^*$, $t \in [0, \varepsilon)$, is a family of functions differentiable in t such that each map $v_h \in S_h^*$ rise to a family of maps $v_h(t) \in S_h^*$ with

$$v_h(t) = v_h + \Psi(t)$$

Basically, a variation of a function $v_h \in S_h^*$ is a modification of its values at each edge midpoint m_i of the simplicial surface M_h given by $v_h(t)(m_i) = v_h(m_i) + \Psi(t)(m_i)$. For simplicity, we restrict to Dirichlet boundary conditions, that is, the variations $\Psi(t)$ are zero at midpoints of boundary edges of M_h .

Definition 66 A critical point v_h in S_h^* of the Dirichlet energy (3.3) in S_h^* with respect to Dirichlet boundary conditions is called a (non-conforming) discrete harmonic map.

Using the identities in an Euclidean triangle T with vertices $\{p_1, p_2, p_3\}$ and oriented edges $\{c_1, c_2, c_3\}$ with $c_i = p_{i-1} - p_{i+1}$, we obtain on T the following representation of the basis functions $\psi_i \in S_h^*$ corresponding to edge c_i :

$$\nabla \psi_i = -2\nabla \varphi_i = \frac{-1}{\text{area } T} J c_i, \quad (3.9)$$

where $\varphi_i \in S_h$ is the conforming basis function corresponding to the triangle vertex p_i opposite to the edge c_i , and J is the rotation of an edge by $\frac{\pi}{2}$ such that Jc points in the opposite direction of the outer normal of the triangle.

Theorem 67 Let $v \in S_h^*$ be a non-conforming function on a simplicial surface M_h . Then the Dirichlet energy of v_h has the explicit representation

$$E_D(v) = \sum_{\text{all edges } c_i} \cot \alpha_i |v_{i-2} - v_{i-1}|^2 + \cot \beta_i |v_{i_1} - v_{i_2}|^2. \quad (3.10)$$

where $\{i_{-2}, i_{-1}, i_1, i_2\}$ denote indices of adjacent edge midpoints as shown in Figure 3.2, and v_{i_j} denotes the value $v(m_{i_j})$. The angles are measured on M_h .

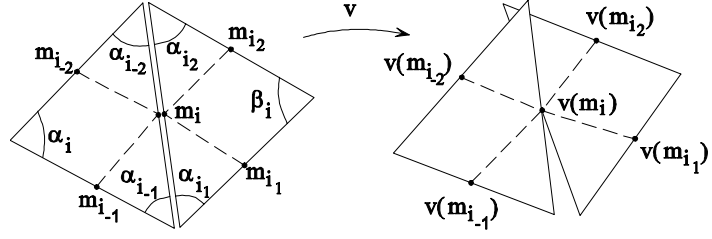


FIGURE 3.2. A non-conforming map is given by its values on edge mid-points.

The unique minimizer of the Dirichlet functional on M_h solves a system of equations such that at each edge midpoint m_i we have

$$\begin{aligned} \frac{d}{dv_i} E_D(v) &= 2(\cot \alpha_{i-2}(v_i - v_{i-1}) + \cot \alpha_{i-1}(v_i - v_{i-2})) \\ &\quad + \cot \alpha_{i+1}(v_i - v_{i+2}) + \cot \alpha_{i+2}(v_i - v_{i+1}) \\ &= 0. \end{aligned} \quad (3.11)$$

Proof. Since $\nabla \psi_i = -2\nabla \varphi_i$, the representation of the Dirichlet energy is a consequence of the explicit representation for conforming elements (3.7). On a single triangle T ,

$$\begin{aligned} E_D(v|_T) &= \frac{1}{2} \int_T - \sum_{j=1}^3 |v_{j+1} - v_{j-1}|^2 \langle \nabla \psi_{j-1}, \nabla \psi_{j+1} \rangle \\ &= \sum_{j=1}^3 \cot \alpha_j |v_{j+1} - v_{j-1}|^2. \end{aligned}$$

The support of a component of the gradient of the Dirichlet energy consists of those two triangles adjacent to the edge corresponding to this variable. Equation (3.11) follows directly from the representation on a single triangle T with edges $\{c_1, c_2, c_3\}$ and $c_1 + c_2 + c_3 = 0$

$$\begin{aligned} \frac{d}{dv_i} E_D(v|_T) &= \int_T \langle \nabla v|_T, \nabla \psi_i \rangle = \frac{1}{\text{area } T} \sum_{j=1}^3 v_j \langle c_j, c_i \rangle \\ &= 2 \cot \alpha_{i-1}(v_i - v_{i+1}) + 2 \cot \alpha_{i+1}(v_i - v_{i-1}) \end{aligned}$$

by combining the expression for the two triangles in the support of ψ_i . \square

3.4 Conjugate Harmonic Maps

Discrete harmonic maps have been well studied as a basic model problem in finite element theory, while the definition of the conjugate of a discrete harmonic map was not completely settled. In this section we are interested in pairs of discrete harmonic maps on a Riemann surface M which are both minimizers of the Dirichlet energy

$$E(u) = \frac{1}{2} \int_M |\nabla u|^2 dx,$$

and are conjugate, i.e. solutions of the Cauchy Riemann equations

$$dv = *du.$$

We note that generically such pairs do not exist in the space of piecewise linear conforming Lagrange finite elements S_h but the problem naturally leads to the space of piecewise linear non-conforming Crouzeix-Raviart elements S_h^* . S_h alone is too rigid to contain the conjugate of a generic discrete harmonic function.

We define the conjugate harmonic maps of discrete harmonic maps in S_h and in S_h^* . A smooth harmonic map $u : M \rightarrow \mathbb{R}$ on an oriented Riemannian surface M and its conjugate harmonic map $u^* : M \rightarrow \mathbb{R}$ solve the Cauchy-Riemann equations

$$du^* = *du$$

where $*$ is the Hodge star operator with respect to the metric in M . In the discrete version, we denote by J the rotation through $\frac{\pi}{2}$ in the oriented tangent space of M , and start with a locally equivalent definition as Ansatz:

Definition 68 *Let $u \in S_h$, respectively S_h^* , be a discrete harmonic map on a simplicial surface M_h with respect to the Dirichlet energies in S_h , respectively S_h^* . Then its conjugate harmonic map u^* is defined by the requirement that it locally fulfills*

$$\nabla u^*|_T = J \nabla u|_T \quad \forall \text{ triangles } T \in M_h. \quad (3.12)$$

The remainder of the section is devoted to prove that the discrete conjugate map is well-defined by showing the closedness of the differential $*du$, and to prove the harmonicity properties of its integral u^* .

To avoid case distinctions we represent each function with respect to the basis functions ψ_i of S_h^* such that on each triangle

$$u|_T = \sum_{i=1}^3 u_i \psi_i,$$

where u_i is the function value of u at the midpoint of edge c_i . We use the same notation for $u|_T^*$, and obtain by Definition 3.12

$$\sum_{i=1}^3 u_i^* \nabla \psi_i = \sum_{i=1}^3 u_i J \nabla \psi_i. \quad (3.13)$$

Lemma 69 *Let T be a triangle with oriented edges $\{c_1, c_2, c_3\}$, $c_1 + c_2 + c_3 = 0$. A pair of linear functions u and u^* related by Equation (3.13), has values at edge midpoints related by*

$$\begin{pmatrix} u_3^* - u_1^* \\ u_3^* - u_2^* \end{pmatrix} = \begin{pmatrix} \cot \alpha_3 (u_2 - u_1) + \cot \alpha_1 (u_2 - u_3) \\ \cot \alpha_3 (u_2 - u_1) + \cot \alpha_2 (u_3 - u_1) \end{pmatrix} \quad (3.14)$$

Proof. The representation (3.9) of $\nabla \psi_i$ converts Equation (3.13) to

$$\sum_{i=1}^3 u_i^* J c_i = \sum_{i=1}^3 u_i c_i.$$

Using $-c_3 = c_1 + c_2$, we express the left side of the above equation as a vector in the span of $\{Jc_1, Jc_2\}$

$$(u_3^* - u_1^*) Jc_1 + (u_3^* - u_2^*) Jc_2 = \sum_{i=1}^3 u_i c_i.$$

If the triangle T is nondegenerate, then the matrix (Jc_1, Jc_2) has rank 2, and scalar multiplication with c_1 and c_2 yields

$$\begin{pmatrix} u_3^* - u_1^* \\ u_3^* - u_2^* \end{pmatrix} = \frac{2}{\text{area}(T)} \sum_{i=1}^3 u_i \begin{pmatrix} \langle c_2, c_i \rangle \\ -\langle c_1, c_i \rangle \end{pmatrix},$$

which easily transforms to Equation (3.14). \square

Now we consider a discrete harmonic map $u \in S_h$ and prove local exactness of its discrete conjugate differential.

Proposition 70 *Let M_h be a simply connected simplicial surface and $u \in S_h$ with $u : M_h \rightarrow \mathbb{R}^d$ an edge continuous discrete harmonic function. Then the discrete Cauchy-Riemann equations (3.12) have a globally defined solution $u^* : M_h \rightarrow \mathbb{R}^d$ with $u^* \in S_h^*$. Two solutions u_1^* and u_2^* differ by an additive integration constant.*

Proof. We define the discrete differential du^* of u^* such that on each triangle T

$$du_{|T}^* := *du_{|T}.$$

Since $u_{|T}$ is a linear map, the conjugate differential $du_{|T}^*$ is well defined and there exists a unique smooth solution $u_{|T}^*$ of the smooth Cauchy-Riemann equations on T , up to an additive constant. By Lemma 69, $u_{|T}^*$ is explicitly given in terms of $u_{|T}$ and T .

If $u \in S_h$ is a discrete harmonic map then it turns out that du^* is closed along closed paths on M_h that cross edges only at their midpoints. Since du^* is closed inside each triangle, it is sufficient to prove closedness for a path γ in the vertex star of a vertex $p \in M_h$ such that $\gamma_{|T}$ linearly connects the midpoints of the two edges of T having p in common, see Figure 3.3. Let $\{m_1, \dots, m_k\}$ be the sequence

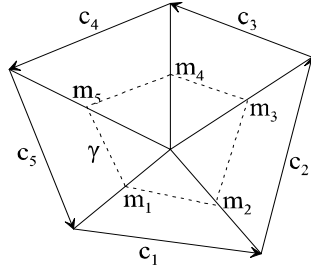


FIGURE 3.3. Dual edge graph γ around a vertex.

of edge midpoints determining γ . The edges $d_j := m_{j+1} - m_j$ of γ are parallel to c_j with $c_j = 2d_j$. We use Equation (3.14) in each triangle to derive

$$\begin{aligned} \int_{\gamma} du^* &= \sum_{j=1}^k \int_{\gamma_{|T_j}} *du_{|T_j} = \sum_{j=1}^k \langle J\nabla u_{|T_j}, d_j \rangle \\ &= -\frac{1}{2} \sum_{j=1}^k \langle \nabla u_{|T_j}, Jc_j \rangle = 0, \end{aligned}$$

since u is harmonic in S_h , see Equation (3.8). Therefore, du^* is closed along the dual edge graph through the edge midpoints of M_h , and $u^* \in S_h^*$ is globally defined on simply connected regions of M_h . \square

For a harmonic map $u \in S_h$, the following proposition proves harmonicity of the conjugate map $u^* \in S_h^*$.

Proposition 71 *Let $u \in S_h$ be a discrete harmonic map on a simplicial surface M_h and let $u^* \in S_h^*$ be a solution of the discrete Cauchy-Riemann equations (3.12) given by Proposition 70. Then u^* has the same Dirichlet energy as u , and u^* is discrete harmonic in S_h^* .*

Proof. Let u^* be the solution of the discrete Cauchy-Riemann equations (3.12) for a discrete harmonic map $u \in S_h$. Then we show that u^* is a critical point of the non-conforming Dirichlet energy in S_h^* by rewriting the Dirichlet gradient (3.11) of u^* in terms of values of u .

On a single triangle T with midpoint m_i on edge c_i , we note that

$$\langle J\nabla u|_T, \nabla \psi_i \rangle = \frac{2}{\text{area } T} (u(m_{i-1}) - u(m_{i+1})) \quad \forall i \in \{1, 2, 3\}, \quad (3.15)$$

which follows directly from $\nabla u = \sum_{j=1}^3 u(m_j) \nabla \psi_j$ and

$$\langle J\nabla \psi_j, \nabla \psi_i \rangle = \begin{cases} 0 & j = i \\ \frac{2}{\text{area}(T)} & j = i - 1 \\ \frac{-2}{\text{area}(T)} & j = i + 1 \end{cases}.$$

Let $T_1 \cup T_2$ denote the two triangles forming the support of ψ_i as shown in Figure 3.4. Using Equation (3.15) we obtain

$$\begin{aligned} \frac{d}{du_i^*} E_D(u^*) &= \int_{T_1 \cup T_2} \langle \nabla u^*, \nabla \psi_i \rangle \\ &= 2(u(m_{i-2}) - u(m_{i-1})) + 2(u(m_{i1}) - u(m_{i2})). \end{aligned}$$

Since u is linear we can rewrite the differences at edge midpoints as differences of u at vertices on the common edge of T_1 and T_2 , and obtain

$$\frac{d}{du_i^*} E_D(u^*) = u(V_{j-1}) - u(V_{j-2}) + u(V_{j2}) - u(V_{j1}). \quad (3.16)$$

This equation relates the energy gradient of u^* to the function values at vertices of u . We emphasize the fact that the derivation of the equation does not use edge continuity of u , which will allow us to use 3.16 in the proof of Theorem 72. The right hand side of (3.16) vanishes if and only if

$$u|_{e_i \text{ in } T_1} = u|_{e_i \text{ in } T_2} + \text{constant}.$$

Therefore, the harmonicity of u^* follows from, and is equal to, the edge continuity of $u \in S_h$. \square

The following main theorem states the complete relationship between harmonic maps in S_h and S_h^* , and includes the previous propositions as special cases.

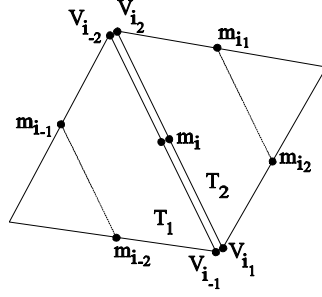


FIGURE 3.4. Notation of edge midpoints in pair of triangles.

Theorem 72 *Let M_h be a simplicial surface in \mathbb{R}^m and S_h respectively S_h^* the space of conforming respectively non-conforming maps from M_h into \mathbb{R}^d . Then we have the following duality of Laplace-Beltrami harmonic maps on M_h :*

1. *Let $u \in S_h$ be a minimizer of the Dirichlet energy in S_h . Then its conjugate map u^* is in S_h^* and is discrete harmonic.*
2. *Let $v \in S_h^*$ be a minimizer of the Dirichlet energy in S_h^* . Then its conjugate map u is in S_h and discrete harmonic.*
3. *Let $u \in S_h$, respectively S_h^* , be discrete harmonic in S_h , respectively S_h^* . Then $u^{**} = -u$.*

Proof. 1. The first statement was proved in Propositions 70 and 71.
 2. Let $v \in S_h^*$ given by $v = \sum v_i \psi_i$ be discrete harmonic. Along the lines of the proof for the corresponding Proposition 70 concerning S_h , we define $v_{|T}^*$ (up to an additive integration constant) as the well-defined integral of

$$dv_{|T}^* := *dv_{|T} \quad \forall T \in M_h,$$

which uniquely exists since $v_{|T}$ is linear. Using the same arguments as in the proof of Proposition 71 and $\nabla v^* = J\nabla v$, we derive an equation for v that is identical to Equation (3.16) for u :

$$\frac{d}{dv_i} E_D(v) = v^*(V_{j-1}) - v^*(V_{j-2}) + v^*(V_{j2}) - v^*(V_{j1}),$$

where V_{j_k} are vertices as denoted in Figure 3.4. Since v is harmonic, we can choose the integration constants of v^* such that v^* becomes edge continuous and lies in S_h .

The harmonicity property of v^* follows from the closedness of v . Let $v^* = \sum v_i^* \varphi_i \in S_h$, and then splitting $\nabla \psi_i = -\nabla \psi_{i_j} - \nabla \psi_{i_{j+1}}$ in each triangle, we obtain

$$\begin{aligned}
\frac{d}{dv_i^*} E_D(v^*) &= \int_{M_h} \left\langle \nabla v^*, \frac{d}{dv_i^*} \nabla v^* \right\rangle = \int_{\text{star}(p_i)} \langle J \nabla v, \nabla \varphi_i \rangle \\
&= \sum_j \int_{T_{i_j}} \left\langle J \nabla v, -\frac{1}{2} (\nabla \psi_{i_j} + \nabla \psi_{i_{j+1}}) \right\rangle \\
&= \sum_j \int_{T_{i_j}} \frac{1}{\text{area } T_{i_j}} ((v_{i_{j+1}} - v_{i_{j-1}}) + (v_{i_{j-1}} - v_{i_j})) \\
&= \sum_j v_{i_{j+1}} - v_{i_j} = 0
\end{aligned}$$

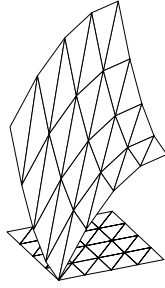
since $v \in S_h^*$ is closed on the path around each vertex p_i . Therefore v^* is critical for the Dirichlet energy in S_h .

3. The third statement is a direct consequence of applying the $*$ operator twice, which rotates the gradient in each triangle by π in the plane of the gradient. \square

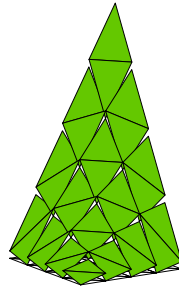
Corollary 73 *Conjugation is a bijection between discrete Laplace-Beltrami harmonic maps in S_h and S_h^* , where each pair (u, v) fulfills the discrete Cauchy Riemann equations. Further, corresponding maps have the same Dirichlet energy.*

Proof. The proof of Theorem 72 and the previous propositions show that, for a pair (u, v) of harmonic conjugate functions $u \in S_h$ and $v \in S_h^*$, the harmonicity condition of u is equal to the closedness condition of v , and the closedness condition of u is equal to the harmonicity condition of v .

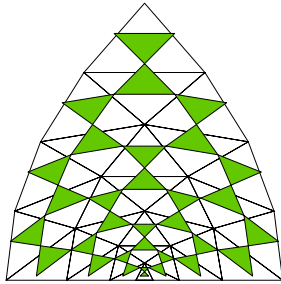
The equality of the Dirichlet energies follows directly from the Cauchy-Riemann equations. \square



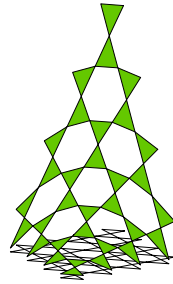
Discrete harmonic map
 $u \in S_h$ interpolating $\operatorname{Re} z^2$



Conjugate harmonic $u^* \in S_h^*$
is a non-conforming map



Holomorphic pair (u, u^*) and
exact solution as full grid



u^* applied to center
quarter of each triangle.

3.5 Minimizing with Conjugate Gradients

For completeness we will mention some of the numerical methods to practically solve the variational problems which we discussed so far. These methods apply to both the conforming and non-conforming meshes.

Let u_h be a map from a simplicial surface M_h satisfying a Dirichlet boundary value problem

$$\begin{aligned} u_h & : M_h \rightarrow \mathbb{R}^3 \\ u_h|_{\partial M} & = \Gamma. \end{aligned}$$

With respect to the Lagrange basis functions, u_h is given

$$u_h(x) = \sum_{i=1}^n u_i \varphi_i(x).$$

Assume, we ordered the set vertices of M_h by interior and boundary vertices $\{p_1, \dots, p_I, p_{I+1}, \dots, p_{I+B}\}$. Then the harmonicity condition at each interior vertex p_j is

$$\begin{aligned} \frac{d}{du_j} E_D(u_h) &= \sum_{i=1}^n u_i \int_{M_h} \langle \nabla \varphi_i, \nabla \varphi_j \rangle \\ &= \sum_{i=1}^I u_i \int_{M_h} \langle \nabla \varphi_i, \nabla \varphi_j \rangle + \sum_{i=I+1}^{I+B} u_i \int_{M_h} \langle \nabla \varphi_i, \nabla \varphi_j \rangle \\ &= 0 \quad \forall j \in \{1, \dots, I\}. \end{aligned}$$

This system of equations is equivalent to a single matrix equation

$$Au = B$$

where $A = (a_{ji})$ is an $I \times I$ matrix, the so-called *stiffness matrix*, and $u = (u_i)$ and $B = (b_j)$ are I dimensional vectors with

$$\begin{aligned} a_{ji} &= \int_{M_h} \langle \nabla \varphi_i, \nabla \varphi_j \rangle \\ b_j &= \sum_{i=I+1}^{I+B} u_i \int_{M_h} \langle \nabla \varphi_i, \nabla \varphi_j \rangle. \end{aligned}$$

In praxis it is usually more efficient not solve the matrix system but employ a conjugate gradient method which is an iterative method with a fast convergence especially during the first iteration steps. See the comments of Brakke [17] who compared our method with other minimization algorithms built into the surface evolver.

The method of *steepest descent* is an iterative algorithm which incrementally reduces the energy by modifying the function u_h a small distance ε in the direction of the negative of the energy gradient

$$\begin{aligned} u_0 &: = u_h \\ u_{i+1} &: = u_i - \varepsilon \nabla E_p(u_i). \end{aligned}$$

The *conjugate gradient method* is a more efficient method where the direction vector is modified such that previous optimizations are not spoiled. It uses a sequence of *line minimizations*: given $p \in \mathbb{R}^n$, direction $n \in \mathbb{R}^n$ and an energy functional $E : \mathbb{R}^n \rightarrow \mathbb{R}$. Find a scalar λ that minimizes

$$E(p + \lambda n) \rightarrow \min,$$

and then replace p by $p + \lambda n$. If the energy functional is differentiable then an obvious choice for a direction is the gradient of E . Such a

gradient method can be more efficient by incorporating second order information which avoids spoiling of previous results.

The Taylor expansion around p gives

$$\begin{aligned} E(x) &= E(p) + \nabla E_p(x) + \frac{1}{2} \nabla^2 E_p(x, x) + \dots \\ &\approx c - bx + \frac{1}{2} x^t A x \end{aligned}$$

For a quadratic function E the gradient can be written as

$$\nabla E(x) = Ax - b.$$

How does the gradient change along some direction ν ?

$$\partial_\nu \nabla E = A \cdot \partial_\nu x = Av$$

The idea of the conjugate gradient method can be summarized as follows: assume we have moved along some direction u to a minimum and now want to move along a new direction v . Then v shall not spoil our previous minimization, i.e. the change of the gradient shall be perpendicular to u :

$$0 = \langle u, \partial_\nu (\nabla E) \rangle = uAv$$

The vectors u and v are called *conjugate directions* which can be constructed using the following Gram-Schmidt bi-orthogonalization procedure employed in the methods of Fletcher-Reeves and Polak-Ribiere [89][102].

Let A be a positive-definite, symmetric $n \times n$ matrix. Let g_0 be an arbitrary vector, and $h_0 = g_0$. For $i = 0, 1, 2, \dots$ define the two sequences of vectors

$$\begin{aligned} g_{i+1} &= g_i - \lambda_i A h_i \\ h_{i+1} &= g_{i+1} + \gamma_i h_i, \end{aligned} \tag{3.17}$$

where λ_i respectively γ_i are chosen to obtain mutually orthogonal vectors $g_{i+1} \cdot g_i = 0$ respectively mutually conjugate directions $h_{i+1} A h_i = 0$, that is:

$$\lambda_i = \frac{g_i \cdot g_i}{g_i A h_i} \quad \gamma_i = -\frac{g_{i+1} A h_i}{h_i A h_i}.$$

If denominators are zero take $\lambda_i = 0$ resp. $\gamma_i = 0$. Then

$$g_i \cdot g_{i+1} = 0 \quad h_i A h_j = 0 \quad \forall i \neq j$$

and the bi-orthogonalization procedure has produced a sequence g_i where each g_i is orthogonal and each h_i is conjugate to its set of predecessors.

Generally, the Hessian matrix A is not known. In this case the following observation provides the essential hints. Assume E is a quadratic functional and we take

$$g_i := -\nabla E|_{p_i} \quad \text{for some point } p_i.$$

Then we proceed from p_i along the direction h_i to the local minimum of E which is located at some point p_{i+1} . If we set again $g_{i+1} := -\nabla E|_{p_{i+1}}$ then this vector g_{i+1} is exactly the vector which would have been obtained by the above Equations 3.17 but without the knowledge of the Hessian A . More precisely, the matrix A never needs to be computed.

Summarizing, the conjugate gradient method computes a set of directions h_i using only line minimizations, the evaluations of the energy gradient, and an auxiliary vector to store the recent vectors g_i . In practice, further optimizations are obtained through pre-conditioning.

3.6 Discrete Laplace Operators

The discretization of the second order Laplace operator for smooth functions to simplicial meshes may be pursued in different ways. Depending on the structure of and information about the underlying mesh the Laplace operator may include more combinatorial or more geometric information. Here we review some basic combinatorial Laplacians and then relate them with the Laplace-Beltrami operator in the context of the functions spaces used in this chapter.

Combinatorial Laplacian

The purely combinatorial point of view ignores metric information like edge length or vertex angles of a mesh. All information about a combinatorial mesh is contained in its connectivity. For theoretical purposes it is convenient to express the connectivity in the form of the adjacency matrix.

Definition 74 *Let $\{p_1, \dots, p_n\}$ be the vertices of a mesh. Then the adjacency matrix A of the mesh connectivity is an $n \times n$ matrix given*

by

$$A_{ij} = \begin{cases} 1 & \text{if } p_i p_j \text{ is an edge} \\ 0 & \text{else} \end{cases}$$

The matrix A is sparse, and the sum of the i -th row respectively column is equal to the valence d_i of the vertex i . Note, in practical applications one would never explicitly store the full matrix.

Definition 75 Let D be an $n \times n$ diagonal matrix with entries $d_{ii} := \frac{1}{d_i}$ where d_i is the valence of the vertex p_i , then the matrix

$$L \quad : \quad = \text{id} - DA$$

$$L_{ij} = \begin{cases} 1 & i = j \\ -\frac{1}{d_i} & \text{if } p_i p_j \text{ is an edge} \\ 0 & \text{else} \end{cases}$$

is the combinatorial Laplacian of the mesh, or short, the mesh Laplacian.

Let e_i be the vector $(0, \dots, 0, 1, 0, \dots, 0)$ with 1 at the i -th position which is associated to p_i . Then

$$Le_i = e_i - \frac{1}{d_i} \sum_{j \in n(i)} e_j$$

where $n(i)$ denotes the set of vertices adjacent to p_i excluding p_i .

Karni and Gotsmann [68] extend the mesh Laplacian in the framework of mesh compression to include distance information

$$GL(p_i) = p_i - \frac{\sum_{j \in n(i)} \frac{1}{|p_i - p_j|} p_j}{\sum_{j \in n(i)} \frac{1}{|p_i - p_j|}}.$$

Five-Point Laplacian

The five-point Laplacian is the $2d$ -extension of the finite difference Laplacian on the real axis. Consider a real-valued function $f : \mathbb{R} \rightarrow \mathbb{R}$ on an interval of the real axis. Then the smooth Laplacian Δf is defined as second derivative of f . In the discrete case, let $\{u_i\}$ be a uniform knot vector on the axis, for example, $u_i := i$, then $f_h''(x_i)$ can be approximated using finite differences

$$\begin{aligned} f_h''(x_i) &= \frac{1}{2} (f_h'(x_i) - f_h'(x_{i-1})) \\ &= \frac{1}{2} ((f(x_{i+1}) - f(x_i)) - (f(x_i) - f(x_{i-1}))) \\ &= \frac{1}{2} (f(x_{i+1}) - 2f(x_i) + f(x_{i-1})) \end{aligned}$$

In explicit notation we have at an interior vertex p and an interior edge midpoint m

$$\begin{aligned}\Delta_h u(p) &= -\frac{1}{2} \sum_{q_i \in n(p)} (\cot \alpha_i + \cot \beta_i)(u(p) - u(q_i)) \\ \Delta_h^* u(m) &= -2(\cot \alpha_{-2}(u(m) - u(m_{-1})) + \cot \alpha_{-1}(u(m) - u(m_{-2})) \\ &\quad + \cot \alpha_1(u(m) - u(m_2)) + \cot \alpha_2(u(m) - u(m_1)))\end{aligned}$$

where $\{q_i\}$ is the set of vertices on the link of p , and $\{m_i\}$ the set of vertices on the link of m in counter-clockwise order and vertex angles α_i opposite to m_i in each triangle.

In Chapter 7 we will see the relationship between the discrete Laplace-Beltrami operators and the divergence operators on vector fields.

3.7 Extension to Bezier Polyomials

Among the important concepts in CAD is the control polygon of piecewise polynomial curves and surfaces which provides an intuitive representation of the shape. For completeness we show how easily the previous concepts extend to a characterization of harmonicity in terms of the control polygon of Bezier triangles. Here we give the notion of the Dirichlet energy of polynomial maps of order n in terms of their Bezier control polygon.

Any polynomial $b^n : T \rightarrow \mathbb{R}^d$ is determined by a triangular Bezier control grid given by vertices $\{b_I\} \subset \mathbb{R}^d$. Using Bernstein basis functions and barycentric coordinates q on T the polynomial b^n has the representation

$$b^n(q) = \sum_{I=|n|} b_I B_I^n(q) \quad (3.20)$$

using the multi-index $I = (i, j, k)$ with $i + j + k = n$. A good introduction is the book by Farin [41].

For the derivation of the Dirichlet energy we denote the difference vector between two adjacent control points by

$$\Delta b_{I+e_j} := b_{I+e_{j+1}} - b_{I+e_{j-1}}.$$

Similarly we introduce a shortcut for difference of Bernstein polynomials

$$\Delta B_{I-e_j}^{n-1} := B_{I-e_{j+1}}^{n-1} - B_{I-e_{j-1}}^{n-1}.$$

Then we have

Lemma 77 *The Dirichlet energy of a Bezier polynomial $b^n : T \rightarrow \mathbb{R}$ be a Bezier polynom given by Equation 3.20 on a triangle $T \in \mathbb{R}^m$ is given by*

$$\frac{1}{2} \int_T |\nabla b^n|^2 = \sum_{j=1}^3 \cot \alpha_j \sum_{\substack{|I|=|J| \\ =n-1}} \langle \Delta b_{I+e_j}, \Delta b_{J+e_j} \rangle B_{IJ}^n \quad (3.21)$$

where α_j are the vertex angles of the domain triangle T , $\{b_I\}$ the Bezier control points of the image, and coefficients

$$B_{IJ}^n := \int_{\Delta_n} B_I^{n-1} B_J^{n-1} dx,$$

integrated over a triangle Δ_n of area $\frac{n^2}{2}$, which depend on the chosen Bernstein basis B_I^n only, and not on b^n and T .

Proof. We define shortcuts

$$d_j := \frac{d}{du_j} \sum_{|I|=n} b_I B_I^n(u(x)) = n \sum_{|I|=n} b_j B_{I-e_j}^{n-1}(u(x)).$$

such that

$$\nabla b^n(u(x)) = \sum_{j=1}^3 d_j \nabla u_j$$

and

$$|\nabla b^n(u(x))|^2 = \sum_{j=1}^3 \left(d_j^2 |\nabla u_j|^2 + 2d_{j-1}d_{j+1} \langle \nabla u_{j-1}, \nabla u_{j+1} \rangle \right). \quad (3.22)$$

Since

$$\sum_{j=1}^3 \nabla u_j = 0$$

we have

$$\begin{aligned} |\nabla u_j|^2 &= |\nabla u_{j-1}|^2 + 2 \langle \nabla u_{j-1}, \nabla u_{j+1} \rangle + |\nabla u_{j+1}|^2 \\ &= - \langle \nabla u_{j-1}, \nabla u_j \rangle - \langle \nabla u_j, \nabla u_{j+1} \rangle. \end{aligned}$$

Inserting this into above Equation 3.22 leads to

$$|\nabla b^n(u(x))|^2 = - \sum_{j=1}^3 (d_{j+1} - d_{j-1})^2 \langle \nabla u_{j+1}, \nabla u_{j-1} \rangle. \quad (3.23)$$

Using

$$\langle \nabla u_{j-1}, \nabla u_{j+1} \rangle = -\frac{\cot \alpha_j}{2 \text{area } T}.$$

and

$$\begin{aligned} & \int_T (d_{j+1} - d_{j-1})^2 dx & (3.24) \\ &= n^2 \int_T \left(\sum_{|I|=n-1} \Delta b_{I+e_j} B_i^{n-1}(u(x)) \right)^2 dx \\ &= n^2 \sum_{\substack{|I|=|J| \\ =n-1}} \langle \Delta b_{I+e_j}, \Delta b_{J+e_j} \rangle \int_T B_I^{n-1} B_J^{n-1} dx \end{aligned}$$

We replace the integration domain T with a triangle Δ_n of area $\frac{n^2}{2}$ such that $\frac{2 \text{area } T}{n^2}$ is factored out and obtain the proposed equation. \square

For each j the double sum contains pairwise scalar products for all parallel edges of the Bezier control net. The independent coefficients B_{IJ}^n and the right-hand integral can be precomputed and stored in a lookup table. They are totally symmetric with respect to any permutation inside I and J .

The Dirichlet energy is quadratic in the control points of the Bezier net. Let $b := (b_1, \dots, b_m)$ be a linear enumeration of all Bezier control points then one can setup a stiffness matrix S such that

$$E_D(b^n) = {}^t B \cdot S \cdot B.$$

The same matrix can be used for the Dirichlet gradient:

Lemma 78 *Let $E_D(b^n)$ be the Dirichlet energy of a Bezier polynomial over a triangle T . By variation of a Bezier control point b_J we obtain the J -th component of the Dirichlet gradient*

$$\frac{d}{db_J} \int_T |\nabla b^n|^2 dx = 4 \sum_{j=1}^3 \cot \alpha_j \sum_{|I|=n-1} \Delta b_{I+e_j} \int_{\Delta_n} B_I^{n-1} \Delta B_{J-e_j}^{n-1} dx.$$

Proof. Using a different numbering in Equation 3.24 we obtain

$$\begin{aligned} \int_T (d_{j+1} - d_{j-1})^2 dx &= n^2 \int_T \left(\sum_{|I|=n} b_I \Delta B_{I-e_j}^{n-1} \right)^2 dx \\ &= n^2 \sum_{|I|=|J|=n} b_I b_J \int_T \Delta B_{I-e_j}^{n-1} \Delta B_{J-e_j}^{n-1} dx \end{aligned}$$

which leads to

$$\begin{aligned}
& \frac{1}{2} \int_T |\nabla b^n(u(x))|^2 dx \\
&= \sum_{j=1}^3 \cot \alpha_j \cdot \sum_{|I|=|J|=n} b_I b_J \int_{\Delta_n} \Delta B_{I-e_j}^{n-1} \Delta B_{J-e_j}^{n-1} dx \\
&= 4 \sum_{j=1}^3 \cot \alpha_j \sum_{|I|=n} b_I \int_{\Delta_n} \Delta B_{I-e_j}^{n-1} \Delta B_{J-e_j}^{n-1} dx.
\end{aligned}$$

The proposed equation follows by inserting the Bezier representation of $\Delta B_{I-e_j}^{n-1}$. \square

4

Discrete Minimal Surfaces

Minimal surfaces are characterized by having least area compared to nearby surfaces with the same boundary. This variational property, which was the original interest in minimal surfaces, was soon relaxed to include unstable critical points as well. Equivalently, these surfaces can be geometrically characterized by having vanishing mean curvature.

Examples have played a central part in the development of the minimal surface theory and fruitfully complemented the theoretical research. In recent years many new examples were studied experimentally using elaborate calculations for the analytic continuation of complex functions and the integration of the Weierstraß representation formulas. Although these methods allow one to compute any surface given by its Weierstraß representation, this analytic approach has the drawback that the Weierstraß formulas must be known in advance. Since the existence of many unstable minimal surfaces was mathematically proved indirectly via the so-called *conjugate surface construction* there was a strong need to develop a numerical scheme and actually compute the conjugate surface of a minimal surface [65][67]. The numerical method developed in [87] jointly with Pinkall was the first scheme to compute the conjugate of a numerically computed minimal surface. The key insight came from a new understanding of the geometric and variational properties of triangle nets. The method

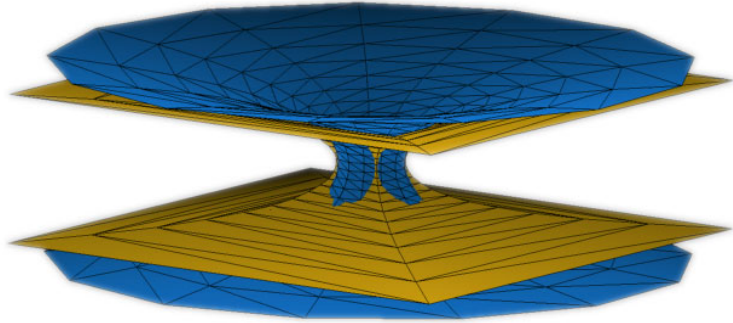


FIGURE 4.1. Asymptotic growth of two complete discrete catenoids depends on the dihedral symmetry.

was later extended in [85] jointly with Oberknapp to the computation of constant mean curvature surfaces via a conjugation of minimal surfaces in \mathbb{S}^3 , compare Chapter 5.

The main theoretical result in this section is a new precise understanding of the variational properties of pairs of discrete conjugate minimal surfaces, which was not known in the original works, by working in the function space of non-conforming triangle meshes. This chapter also introduces discrete minimal surfaces and derives their variational properties, we define the mean curvature normal as an operator on the discrete mesh.

Another important result is an explicit description of some complete discrete minimal surfaces which were jointly discovered with Rossman [97]. For example, these descriptions allow one to construct unstable discrete surfaces whose shape is given by exact coordinates, a fact which is particularly useful for the study of higher order properties like the index of minimal surfaces, see Chapter 6.

4.1 Review of the Smooth Variation of Area

Let $F : \Omega \rightarrow M \subset \mathbb{R}^3$ be a parameterized surface of a domain $\Omega \subset \mathbb{R}^2$. A variation of M is a family of surfaces given by a differentiable map

$$\begin{aligned} G : \Omega \times (-\varepsilon, \varepsilon) &\rightarrow \mathbb{R}^3 \\ G(x, 0) &= F(x) \quad x \in \Omega. \end{aligned}$$

The induced vector field on M

$$\begin{aligned} Y & : \quad \Omega \rightarrow TM \\ Y(x) & = \quad \frac{d}{d\varepsilon} G(x, \varepsilon)|_{\varepsilon=0} \end{aligned}$$

is called the *first variation* of G .

Lemma 79 *For a given surface M and a variation vector field Y the first variation of the area functional at M in the direction of Y is defined by*

$$\delta \text{area}(M, Y) := \frac{d}{d\varepsilon} \text{area}(M_\varepsilon)|_{\varepsilon=0} \in \mathbb{R}$$

and given by

$$-\delta \text{area}(M, Y) = \int_{\partial M} \langle Y, \nu \rangle ds + 2 \int_M \langle Y, N \rangle H dA ,$$

where ν is the outer normal along ∂M .

Proof. see Hildebrandt et al. [31] or Lawson [72]. \square

If $Y = \lambda N$ is a normal variation then the boundary component vanishes and we have

$$\delta \text{area}(M, Y) = -2 \int_M \lambda H dA.$$

Further, if $\lambda \equiv 1$ and H is constant we obtain

$$H = -\frac{\delta \text{area}(M, N)}{\text{area}(M)}.$$

4.2 First Variation of the Discrete Area and Volume

A variation of a polyhedral surface is determined by a variation of its vertices with the same mesh connectivity. For simplicity we require a C^2 variation but often a differentiability of lower order is sufficient.

Definition 80 *Let $\mathcal{P} = \{p_1, \dots, p_m\}$ be the set of vertices of a discrete surface M_h . A variation $M_h(t)$ of M_h is defined as a C^2 variation of the vertices p_i*

$$p_i(t) : [0, \varepsilon) \rightarrow \mathbb{R}^d \quad \text{so that} \quad p_i(0) = p_i \quad \forall i = 1, \dots, m.$$

The straightness of the edges and the flatness of the triangles are preserved as the vertices move.

Formally, we have for each t that $p_i(t) \in S_h$ and $p_i(0) = id(M_h)$ is the identity map of M_h .

Up to first order a variation is given by a set of vectors $\mathcal{V} = \{v_1, \dots, v_m\}$, $v_i \in \mathbb{R}^d$ defined on the vertices $\mathcal{P} = \{p_1, \dots, p_m\}$ of M_h . Often we restrict a variation to interior vertices by assuming $v_i = 0 \in \mathbb{R}^d$ along the boundary, or add special constraints on the boundary of M_h . The vectors v_{p_j} are the *variation vector field* such that the variation has the form

$$p_j(t) = p_j + t \cdot v_{p_j} + \mathcal{O}(t^2), \quad (4.1)$$

that is, $p_j'(0) = v_{p_j}$. We define the vector $\vec{v} \in \mathbb{R}^{dm}$ by

$$\vec{v} = (v_1^t, \dots, v_m^t). \quad (4.2)$$

In the following we will restrict to $d = 3$ which allows the use of a well-defined normal vector although many results hold in higher codimension too.

In the smooth situation, the variation at interior points is typically restricted to normal variation since the tangential part of the variation only performs a reparametrization of the surface. However, on discrete surfaces there is an ambiguity in the choice of normal vectors at the vertices, so we allow arbitrary variations. But we will later see in Chapter 6 (Section 6.5) that our experimental results can accurately estimate normal variations of a smooth surface when the discrete surface is a close approximation to the smooth surface.

In the following we derive the evolution equations for some basic discrete operators under variation $M_h(t)$ of a discrete surface M_h .

Recalling, that the area of a discrete surface is

$$\text{area } M_h := \sum_{T \in \mathcal{T}} \text{area } T,$$

where $\text{area } M_h$ denotes the Euclidean area of the triangle T as a subset of \mathbb{R}^3 .

At each vertex p of M_h , the gradient of area is

$$\nabla_p \text{area } M_h = \frac{1}{2} \sum_{T=(p,q,r) \in \text{star } p} J(r-q), \quad (4.3)$$

where J is rotation of angle $\frac{\pi}{2}$ in the plane of each oriented triangle T . The first derivative of the surface area is then given by the chain

rule

$$\frac{d}{dt} \text{area } M_h = \sum_{p \in \mathcal{V}} \langle p', \nabla_p \text{area } M_h \rangle. \quad (4.4)$$

The volume of an oriented surface M_h is the oriented volume enclosed by the cone of the surface over the origin in \mathbb{R}^3

$$\text{vol } M_h := \frac{1}{6} \sum_{T=(p,q,r) \in M_h} \langle p, q \times r \rangle = \frac{1}{3} \sum_{T=(p,q,r) \in M_h} \langle \vec{N}, p \rangle \cdot \text{area } T,$$

where p is any of the three vertices of the triangle T and $\vec{N} = (q - p) \times (r - p) / |(q - p) \times (r - p)|$ is the oriented normal of T . It follows that

$$\nabla_p \text{vol } M_h = \sum_{T=(p,q,r) \in \text{star } p} q \times r / 6 \quad (4.5)$$

and

$$\frac{d}{dt} \text{vol } M_h = \sum_{p \in \mathcal{P}} \langle p', \nabla_p \text{vol } M_h \rangle. \quad (4.6)$$

Remark 81 *Note also that $\nabla_p \text{vol } M_h = \sum_{T=(p,q,r) \in \text{star } p} (2 \cdot \text{area } T \cdot \vec{N} + p \times (r - q)) / 6$. Furthermore, if p is an interior vertex, then the boundary of $\text{star } p$ is closed and $\sum_{T \in \text{star } p} p \times (r - q) = 0$. Hence the $q \times r$ in Equation 4.5 can be replaced with $2 \cdot \text{area } T \cdot \vec{N}$ whenever p is an interior vertex.*

4.3 Discrete Mean Curvature

The mean curvature vector on smooth surfaces provides a measure how much the surface area changes compared to near-by surfaces, that means, if a surface is moved at constant speed along the surface normal. In the polyhedral case we will use a similar approach to obtain a discrete version of the mean curvature vector. Similar to the definition of a discrete Gauß curvature the polyhedral mean curvature will measure the curvature of a small region. Later it will turn out that the mean curvature vector can be interpreted as the discrete Laplace-Beltrami operator on surfaces which was introduced in Chapter 3.

The area of a polyhedral surface is defined as the sum of the area of all elements. Let T be a triangle spanned by two edges v and w emanating from a vertex then its area is given by the relation $4 \text{area}^2 T = |v|^2 |w|^2 - \langle v, w \rangle^2$. In the following we prefer an expression

of the area in terms of vertices and vertex angles of the surface. Let T be a triangle with vertices q_i and vertex angles α_i . Then

$$\text{area } T = \frac{1}{4} \sum_{j=1}^3 \cot \alpha_j |q_{j-1} - q_{j+1}|^2. \quad (4.7)$$

For practical applications we derive a simple formula of the area gradient in intrinsic terms of the polyhedral mesh, see [87].

Lemma 82 *Let p be an interior vertex of a simplicial surface M_h . Then the gradient of the area with respect to variation of vertices can be expressed in the following cotangent formula*

$$\nabla_p \text{area } M_h = \frac{1}{2} \sum_j (\cot \alpha_j + \cot \beta_j)(p - q_j). \quad (4.8)$$

Proof. The area gradient is the sum of the individual area gradients of all triangles containing p . In each triangle the area gradient of p is parallel to the height vector point toward p with length $|c|$. If c is the oriented edge opposite to p and J the rotation in the oriented plane of the triangle by $\frac{\pi}{2}$ then the gradient can be expressed by $\frac{1}{2}Jc$. Summing over all triangles containing p we obtain

$$\nabla_p \text{area } M_h = \frac{1}{2} \sum_j Jc_j.$$

Using the explicit representation of Jc on a single triangle with edges $c = a - b$ and vertex angles α and β at the end points of c ,

$$Jc = a \cot \alpha + b \cot \beta,$$

one obtains the proposed equation. \square

This formula easily generalizes to non-manifold surfaces where, for example, three triangles join at a common edge.

If $M_h(t)$ is a variation of simplicial surfaces such that each vertex $p(t)$ is a differentiable function for $t \in (-\varepsilon, \varepsilon)$ then

$$\frac{d}{dt} \text{area } M_h(t) = \sum_{p \in P} \langle p', \nabla_p \text{area } M_h \rangle.$$

The mean curvature of a smooth surface measures the variation of area when changing to parallel surfaces in normal direction. In the discrete case there exists no unique normal vector, but, as first derived in [87], if we choose as normal vector the direction of the area gradient, then the following definition leads to a discrete mean curvature vector which has similar properties as the smooth mean curvature vector.

Definition 83 *The discrete mean curvature at the vertex p of a simplicial surface M_h is a vector-valued quantity*

$$\vec{H}(p) := \nabla_p \text{area } M_h. \quad (4.9)$$

Note that this mean curvature operator is an integrated operator and measures the total mean curvature in the vicinity of a vertex. Therefore, when computing the total mean curvature of a surface one simply needs to sum up the mean curvature of all vertices instead of integrating over the surface. In this sense, the mean curvature is a measure at vertices similar to the (total) Gauss curvature introduced in Definition 19. Compare the definition of discrete mean curvature by Hsu, Kusner and Sullivan [62] in the experimental study of minimizers of the Willmore integral.

Another idea, which we just mention for completeness, is to define the mean curvature at edges instead of vertices based on the heuristic that the bending of a surface happens at edges. Here we will compare these two approaches.

Lemma 84 *Let e be an edge common to two triangles T_1 and T_2 , and let m be an arbitrary point in the interior of e . If we bisect both triangles with edges from m and to the vertex opposite to e in each triangle then m becomes a vertex with four adjacent triangles. Then the area gradient at m*

$$\nabla_m \text{area}(\text{star } m) = |e| \cos \frac{\theta}{2} \cdot N_e$$

does not depend on the position of m within the edge but depends only on the dihedral angle θ of the edge, the length of the edge e and the angle bisecting unit normal vector N_e .

Proof. Denote the edges of the triangle T_i with $\{a_i, b_i, e\}$. Then star m consists of four triangles, and we calculate the mean curvature normal at m :

$$\begin{aligned} \nabla_m \text{area}(\text{star } m) &= \frac{1}{2} (J_1 a_1 + J_1 b_1 + J_2 a_2 + J_2 b_2) \\ &= \frac{1}{2} (J_1 e + J_2 e) = |e| \cos \frac{\theta}{2} \cdot N_e \end{aligned}$$

where θ is the edge angle and N_e is the angle bisecting unit normal along e . \square

Since the area gradient is independent of the position of the point m on the edge we use the result of the previous lemma to define the mean curvature of an edge:

Definition 85 Let e be an edge of a simplicial surface M_h . Then the mean curvature vector of the edge is defined by

$$\vec{H}(e) = |e| \cos \frac{\theta}{2} \cdot N_e$$

where θ is the dihedral angle between the two triangles adjacent to e and N_e is the angle bisecting unit normal vector. If e is a boundary edge, we set $\theta := 0$ and $N_e := J_e$.

Note, the sign of the mean curvature is hidden in the definition of the normal vector N_e . If the surface is orientable then one could use a normal vector field and obtain a scalar $H(e)$ whose sign is the sign of $\langle N_e, N \rangle$.

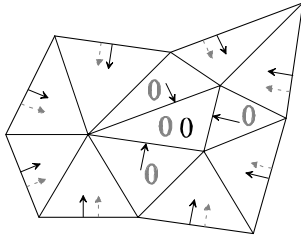
Lemma 86 Let M_h be a simplicial surface possibly with boundary, and let us denote all edges as interior which are not part of the boundary. Then we have

$$\frac{1}{2} \sum_{e \in \partial M_h} J_e = \sum_{e \in \overset{\circ}{M}_h} \vec{H}(e).$$

Proof. The contribution of each triangle, which does not contain a boundary edge, to the total mean curvature term is zero. The contribution of each boundary triangle to the total mean curvature term is equal to the contribution of the left hand side. \square

The following lemma compares the vertex and edge based mean curvature notions.

Lemma 87 Let $\Omega \subset M_h$ be a simply connected domain on a simplicial surface which is a subcomplex and whose boundary $\partial\Omega$ is an embedded circle. Then the total mean curvature of all interior vertices of Ω is equal to the force along the boundary, i.e.



Total mean curvature.

$$\sum_{p \in \overset{\circ}{\Omega}} \vec{H}(p) = \frac{1}{2} \sum_{e \in \partial\Omega} J_e + \text{contribution from vertices.}$$

where the right summation is taken over all edges e of the boundary.

Proof. The margin figure shows the contribution to the total interior mean curvature and the force along the boundary. The black arrows and zeros are the contribution of the edges to the total mean curvature of all interior vertices. The grey arrows and zeros is the contribution to the total mean curvature of all edges. \square

Surface Tension as Force

An equivalent characterization of discrete minimal surfaces is possible by looking at the force which acts on the boundary of a soap film. As in the smooth case we assume at each vertex a tension respectively force. Here the force is assumed to be orthonormal to the edge of the link of a vertex and pointing in outward direction of the triangle.

Definition 88 Let M_h be simplicial surface possibly with boundary. For each vertex $p \in M_h$ we define the force $F(p)$ as the sum of the area gradients of each triangle in star p

$$F(p) := - \sum_{T \in \text{star } p} \nabla_p \text{area } T.$$

Similar to the smooth case the total mean curvature of all interior vertices of a domain on a simplicial surface can be expressed as a boundary term.

Lemma 89 Let M_h be a connected region on a simplicial surface. Then the total mean curvature of all interior points of M_h is equal to the total force along the boundary, i.e.

$$\sum_{p \in \overset{\circ}{M}_h} \vec{H}(p) = \sum_{p \in \partial M_h} F(p).$$

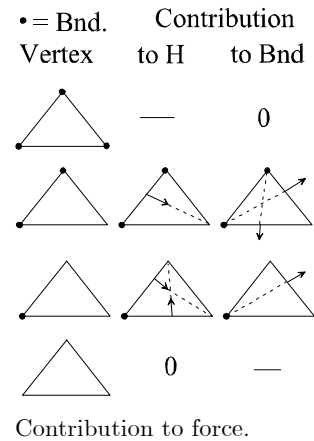
Proof. The margin figure shows the contribution of vertex gradients of the different types of triangles to the total interior mean curvature and to the total force along the boundary.

First, the contribution of triangles with only interior or only boundary triangles is zero for mean curvature and for force. A triangle with one interior vertex contributes the same to the interior vertex as to the two boundary vertices, and a triangle with two interior vertices also has identical contributions. This proves the statement. \square

Therefore, the definition of a discrete minimal surface is equivalent to the vanishing of the total force of the star of each interior vertex, or more general.

Corollary 90 Let M_h be a simplicial surfaces. Then M_h is a discrete minimal surface if and only if the total force vanishes along the boundary of any connected region $\Omega \subset M_h$ vanishes.

Proof. If M_h is minimal then the total interior mean curvature of any region Ω in M_h is zero and by Lemma 89 the total force of $\partial\Omega$ vanishes. The minimality of M_h follows from the vanishing of the force of the link of each vertex star. \square



4.4 Properties of Discrete Minimal Surfaces

In the previous section we have introduced the notion of mean curvature vector as the gradient of the discrete area functional. Here we will study the critical values of the area functional in more detail, that is, surfaces with $H \equiv 0$.

Definition 91 *A simplicial surface M_h is a discrete minimal surface iff the discrete area functional of M_h is critical w.r.t. variations of any set of interior vertices. To include symmetry properties into this definition we sometimes allow a constrained variation of boundary points:*

- *if a boundary arc is a straight line, then its interior points may vary along the straight line*
- *if a boundary arc is a planar curve, then its interior points may vary within the plane*
- *in all other cases the boundary points always remain fixed.*

Note that the above definition is equivalent to saying that the area of M_h is critical with respect to variations of any interior vertex. The relaxed boundary constraints allow us to simulate free boundary value problems, and to extend minimal surfaces by reflection.

Corollary 92 *A simplicial surface M_h is minimal if and only if at each interior vertex p*

$$\nabla_p \text{area } M_h = \frac{1}{2} \sum_j (\cot \alpha_j + \cot \beta_j)(p - q_j) = 0 \quad (4.10)$$

where $\{q_j\}$ denotes the set of vertices of link p and α_j, β_j denote the two angles opposite to the edge pq_j . At boundary vertices on symmetry arcs the area gradient is constraint to be tangential to the straight line or to the plane.

Proof. This equation follows directly from the representation of the area gradient as the discrete mean curvature vector. \square

The following properties of discrete minimal surfaces derived in [87] are similar to equivalent properties of harmonic maps.

Lemma 93 *Let M_h be a discrete minimal surface. If the star of an interior vertex p consists of congruent isosceles triangles then p lies in the center of mass of the vertices of its link.*

Proof. The weights in Equation 4.10 are all equal, therefore, p is the mean of its adjacent vertices $\{q_i\}$. \square

The convex hull property for discrete minimal surfaces holds as long as the surface consists only of acute triangles.

Lemma 94 *Let M_h be a discrete minimal surface. If the star of an interior vertex p consists of acute triangles then p lies in the convex hull of its star.*

Proof. The weights in Equation 4.10 are all positive, therefore, p is a convex combination of its adjacent vertices $\{q_i\}$

$$p = \frac{\sum_j (\cot \alpha_j + \cot \beta_j) q_j}{\sum_j (\cot \alpha_j + \cot \beta_j)}$$

and lies within the convex hull of its link spanned by $\{q_i\}$. \square

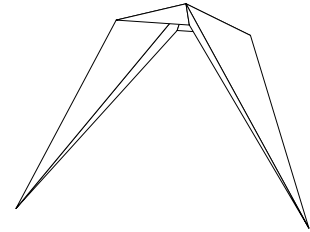
The previous lemma does not hold in a more general case. The following configuration is a counterexample to the maximum principle and the convex hull property of discrete minimal surfaces. Its construction in [94] jointly with Rossman is based on the existence of obtuse triangles. See also the model at [95] which contains an interactive applet to analyze the dependence on the boundary configuration.

The counterexample is a special configuration of the 1-parameter family of discrete minimal surfaces:

```

<points>
  <p>-u 0 -u </p>
  <p> u 0 -u </p>
  <p>-1 1 0 </p>
  <p> 1 1 0 </p>
  <p>-1 -1 0 </p>
  <p> 1 -1 0 </p>
  <p> 0 0 h(u)</p>
</points>
<faces>
  <f>0 6 2</f>
  <f>6 3 2</f>
  <f>6 1 3</f>
  <f>0 4 6</f>
  <f>4 5 6</f>
  <f>5 1 6</f>

```



Counterexample to the maximum principle of discrete minimal surfaces. The center vertex lies outside the convex hull of its link.

</faces>

The parameter u varies in $(0, \infty)$ and the function $h(u)$ determines the vertical height of the center vertex. For $u \in [0, 2]$ the central vertex lies within the convex hull of the boundary after minimization. The remarkable fact is that this property does not hold for $u > 2$ when the minimum position of the central vertex is outside the convex hull of the boundary. The model in the margin figure corresponds to the parameter value $u = 5$.

Note that since the identity map of a discrete minimal surface is a discrete harmonic map, this example also demonstrates that the mean value property and convex hull property of discrete harmonic maps do not hold. Further note that both properties hold in special situations where all triangles have all vertex angles in $[-\frac{\pi}{2}, \frac{\pi}{2}]$. In this example, the center vertex lies on the convex hull exactly at $u = 2$ which is the situation when the first vertex angle becomes $\frac{\pi}{2}$. Increasing u further leads to an increasing angle.

Note that the discrete maximum principle does hold for the five-vertex Laplacian defined over the special rectangular $\mathbb{Z} \times \mathbb{Z}$ grid [20].

4.5 Computing Discrete Minimal Surfaces

A direct minimization of the area functional is a non-linear problem because of the angle terms in Equation 4.10. Another effect, which may spoil numerical convergence, is the invariance of the area functional with respect to reparametrizations of the image surface. This may lead to tangential motions in an area minimization procedure.

The following observation leads to an effective method for area minimization which in fact minimizes the Dirichlet energy in an iteration process. This method was first employed by Dziuk [35] for the mean curvature flow and later used in the context of discrete minimal surfaces by Pinkall and Polthier [87]. For a smooth map $F : M \rightarrow \mathbb{R}^3$ from a Riemann surface M we have the estimate

$$\text{area } F(M) \leq \frac{1}{2} \int_M |\nabla F|^2 dx =: E_D(F)$$

with equality iff F is a conformal map. Following a proposal of Hutchinson [64] we call the difference

$$E_C(F) := E_D(F) - \text{area } F(M)$$

the *conformal energy* of the map F since for a Euclidean (x, y) -domain Ω one has

$$E_C(F) = \frac{1}{2} \int_{\Omega} |JF_x - F_y|^2, \quad (4.11)$$

where J is the rotation by $\frac{\pi}{2}$ in the oriented tangent plane. E_C is a natural measure of failure for a map to be conformal. In the following we will introduce a discrete analogue of these relationships.

Lemma 95 *The gradient of the Dirichlet energy of the identity map id of a simplicial surface M_h is equal to the area gradient, that is, at any interior vertex $p \in M$ we have*

$$\nabla_p \text{area } M_h = \nabla_p E_D(\text{id}).$$

Proof. The statement follows directly by applying the theorem 55 to the id map and comparing its Dirichlet gradient with the area gradient of M_h . \square

Corollary 96 *A simplicial surface M_h is minimal if and only if the identity map $\text{id}_h : M_h \rightarrow M_h$ is discrete harmonic.*

As a consequence, we have a simplicial equivalent for the conformal energy of smooth maps given in Equation 4.11.

Definition 97 *Let $F_h : M_h \rightarrow N_h$ be a map between two simplicial surfaces, then its discrete conformal energy is given by*

$$E_C(F_h) := E_D(F_h) - \text{area } F_h(M_h). \quad (4.12)$$

Corollary 98 *Let $F_h : M_h \rightarrow N_h$ be a map between two simplicial surfaces, then the discrete conformal energy and its gradient are*

$$E_C(F_h) = \frac{1}{4} \sum_{p_i p_j \text{ is edges}} (\Delta\alpha_{ij} + \Delta\beta_{ij}) |F_h(p_i) - F_h(p_j)|^2$$

$$\nabla_{F_h(p_i)} E_C(F_h) = \frac{1}{2} \sum_{p_j \in \text{link } p_i} (\Delta\alpha_{ij} + \Delta\beta_{ij})(F_h(p_i) - F_h(p_j)) \quad (4.13)$$

with the shortcuts

$$\begin{aligned} \Delta\alpha_{ij} & : = \cot \alpha_{ij} - \cot \overline{\alpha}_{ij} \\ \Delta\beta_{ij} & : = \cot \beta_{ij} - \cot \overline{\beta}_{ij} \end{aligned}$$

where α, β denote vertex angles on M_h and $\overline{\alpha}, \overline{\beta}$ denote vertex angles on N_h in triangles opposite to the edge $p_i p_j$.

Proof. The relations follow immediately from the expressions of the discrete area in equation 4.7

$$\nabla_{F_h(p_i)} \text{area } F_h(M_h) = \frac{1}{2} \sum_{p_i p_j \text{ is edges}} (\cot \overline{\alpha_{ij}} + \cot \overline{\beta_{ij}}) (F_h(p_i) - F_h(p_j))$$

and the Dirichlet energy in Theorem 55

$$\nabla_{F_h(p_i)} E_D F_h(M_h) = \frac{1}{2} \sum_{p_i p_j \text{ is edges}} (\cot \alpha_{ij} + \cot \beta_{ij}) (F_h(p_i) - F_h(p_j)).$$

□

Note, a map has vanishing conformal energy if and only if angles of domain and image triangles are equal. But critical values of the conformal energy are much less constrained. For example, Hutchinson [64] noticed that minimizing the conformal energy leads to nice triangulations since it avoids decreasing the surface area which occurs when minimizing the Dirichlet energy.

The following algorithm uses a sequence of discrete harmonic maps. In short, let M_0 be an initial simplicial surface and let a sequence of simplicial surfaces $\{M_i\}$ be defined as images of a sequence of maps

$$\begin{aligned} F_i & : M_i \rightarrow M_{i+1} \\ \Delta_h F_i & = 0 \\ \partial F_i(M_i) & = \Gamma \end{aligned}$$

which are discrete harmonic on M_i . If the limit surface $M := \lim M_i$ exists then the limit function $F : M \rightarrow M$ is harmonic and conformal, therefore, $F(M)$ is minimal.

The algorithm makes essential use of the fact that minimizing the Dirichlet energy also minimizes the surface area in first order. The major advantages of minimizing the Dirichlet energy compared to minimizing surface are, first, that the minimization process has a unique solution, and, second, that tangential motions can be ignored during the first iterations. Compare the comments of Brakke on this issue [17].

Algorithm 99 *Solve the boundary value problem for discrete minimal surfaces (either Dirichlet or Neumann conditions):*

1. Choose an arbitrary initial surface M_0 with boundary $\partial M_0 = \Gamma$ as the first approximation of M , set i to 0.

2. Let M_i be a surface with boundary Γ , then compute the surface M_{i+1} as minimizer of the Dirichlet energy

$$\int_{M_i} |\nabla(F_i : M_i \rightarrow M_{i+1})|^2 = \min_{M, \partial M = \Gamma} \int_{M_i} |\nabla(F : M_i \rightarrow M)|^2.$$

This uniquely defines a Laplace-Beltrami harmonic function F_i whose image $F_i(M_i) = M_{i+1}$ will be taken as the domain surface in the next iteration.

3. Set i to $i + 1$ and continue with step 2, for example, until $|\text{area } M_i - \text{area } M_{i+1}| < \epsilon$.

In practice, this algorithm converges very quickly during the first iteration steps. It slows down if the surface is close to a critical point of the area functional probably because then the area gradient no longer approximates a "good" surface normal. In any case, if the algorithm converges to a non-degenerated surface then the limit is discrete minimal. The next convergence statement shown in [87] is merely a theoretical observation, rather than having use in practical applications since the degeneracy assumption can hardly be ensured in advance.

Proposition 100 *The algorithm converges to a solution of the problem, if no triangles degenerate.*

Proof. The condition "no triangles degenerate" means that we assume all triangle angles for all surfaces of the sequence to be uniformly bounded away from 0 and π . From the construction the sequences $\{\text{area } M_i\}$ and $\{E_D(F_i : M_i \rightarrow M_{i+1})\}$ are monotone decreasing:

$$\begin{aligned} \text{area } M_i = E_D(id|_{M_i}) &\geq E_D(F_i : M_i \rightarrow M_{i+1}) \\ &= \text{area } M_{i+1} + E_C(F_i) \\ &\geq E_D(id|_{M_{i+1}}) = \text{area } M_{i+1}. \end{aligned}$$

If no triangles degenerate we minimize in a compact set of surfaces. Therefore, a subsequence of $\{M_i\}$ converges uniformly to a limit surface M with respect to the norm assumed in the space of surfaces.

Since the identity map of the limit surface M is discrete harmonic the area gradient of M vanishes everywhere, and that means M is discrete minimal. \square

Other Methods for Solving the Plateau Problem

The Plateau problem looks for a minimal surface M spanned by a given boundary curve $\Gamma \subset \mathbb{R}^3$. As an overview we mentioned three popular methods to compute a numerical solution.

Minimal graph: If the surface is known to be a graph over a plane, then there exists a scalar valued function z over a planar domain $\Omega \subset \mathbb{R}^2$ with boundary $\partial\Omega$

$$\begin{aligned} z & : \quad \Omega \rightarrow \mathbb{R} \\ z|_{\partial\Omega} & = \quad g_1 \text{ or} \\ \partial_\nu z|_{\partial\Omega} & = \quad g_2 \end{aligned}$$

where g_1 are prescribed Dirichlet boundary values, or g_2 are Neumann boundary conditions which prescribe the directional derivative of z in direction of the outer normal along $\partial\Omega$. Such a graph is area minimizing w.r.t. to variations with compact support if it fulfills a nonlinear elliptic partial differential equation, the minimal surface equation [31]

$$(1 + z_y^2)z_{xx} - 2z_x z_y z_{xy} + (1 + z_x^2)z_{yy} = 0$$

Mean curvature flow allows us to gradually decrease surface area. Let $M(t)$ with $\partial M(t) = \Gamma$ be a 1-parameter family of C^2 surfaces which is differentiable in t . Then $M(t)$ flows by mean curvature if it fulfills the following parabolic partial differential equation

$$\frac{\partial}{\partial t} M(t) = H(t) \cdot N(t) = \Delta_g M$$

where $H(t)$ is the mean curvature and $N(t)$ the surface normal of $M(t)$. If the flow does not run into a singularity and if it stops, then this limit surface is minimal.

4.6 Conjugate Pairs of Discrete Minimal Surfaces

Here we combine the results on non-conforming meshes of Chapter 3 and on simplicial minimal surfaces to derive the variational properties of pairs of conjugate discrete minimal surfaces.

Review of Smooth Minimal Surfaces

Among the fundamental observations in the theory of smooth minimal surfaces was the fact that each minimal surface comes in a family of minimal surfaces, the so-called *associate family* or *Bonnet family*.

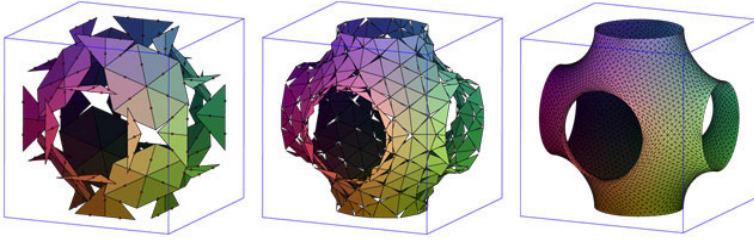


FIGURE 4.2. Free-boundary value problem of Schwarz P-surface in a cube solved via discrete conjugate surface construction. Even the very coarse resolution of the non-conforming mesh gives qualitatively good results.

The simplest and most known example is the associate family which transforms the catenoid C into the helicoid H , both are given by

$$C(u, v) = \begin{pmatrix} \cos v \cosh u \\ \sin v \cosh u \\ u \end{pmatrix}, \quad H(u, v) = \begin{pmatrix} \sin v \sinh u \\ -\cos v \sinh u \\ v \end{pmatrix}.$$

Their associate family $F^\varphi(u, v)$ consists of all minimal surfaces given by

$$F^\varphi(u, v) = \cos \varphi \cdot C(u, v) + \sin \varphi \cdot H(u, v).$$

The surface $F^{\frac{\pi}{2}}$ is called the *conjugate surface* of F^0 , and more general, all pairs F^φ and $F^{\varphi+\frac{\pi}{2}}$ are conjugate to each other. Applying the conjugate twice leads to $F^\pi = -F$ which is obtained from F^0 by reflection in the origin.

A more appropriate notation of the associate family follows from the representation of minimal surfaces as complex curves in \mathbb{C}^3 . Recall the basic fact in minimal surface theory that the three coordinate functions $F = (f_1, f_2, f_3)$ of a minimal surface $F : \Omega \subset \mathbb{R}^2 \rightarrow \mathbb{R}^3$ are harmonic maps if F is a conformal parameterization. Therefore, there exist three conjugate harmonic maps f_i^* which describe another minimal immersion $F^* = (f_1^*, f_2^*, f_3^*) : \Omega \subset \mathbb{R}^2 \rightarrow \mathbb{R}^3$. If we introduce complex coordinates $z = u + iv$ in Ω then combination of both maps to a holomorphic curve $F + iF^* : \Omega \rightarrow \mathbb{C}^3$ with holomorphic coordinate functions gives a family of immersions $F^\varphi = \operatorname{Re}(e^{-i\varphi} \cdot (F + iF^*))$ called the associate family of F or of F^* . In the above example the introduction of complex coordinates leads to the following representation of the associate family of catenoid and helicoid given by

$$F^\varphi(z) = \operatorname{Re}(e^{-i\varphi} \cdot (C(z) + i \cdot H(z))) = \operatorname{Re}(e^{-i\varphi} \cdot \begin{pmatrix} \cosh z \\ -i \sinh z \\ z \end{pmatrix}).$$

The following theorem summarizes the most important properties of the associate family of smooth minimal surfaces without proof.

Theorem 101 *Let $C, H : \Omega \rightarrow \mathbb{R}^3$ be a pair of conformally parametrized conjugate minimal surfaces. Then the associate family $F^\varphi : \Omega \rightarrow \mathbb{R}^3$ has the following properties:*

1. *All surfaces F^φ of the associate family are minimal and isometric.*
2. *The surface normal at each point $F^\varphi(u, v)$ is independent of φ .*
3. *The partial derivatives fulfill the following correspondence:*

$$\begin{aligned} F_u^\varphi(u, v) &= \cos \varphi \cdot C_u(u, v) - \sin \varphi \cdot C_v(u, v) \\ F_v^\varphi(u, v) &= \sin \varphi \cdot C_u(u, v) + \cos \varphi \cdot C_v(u, v) \end{aligned} \quad ,$$

in particular, the partials of a conjugate pair C and H satisfy the Cauchy-Riemann equations:

$$\begin{aligned} C_u(u, v) &= H_v(u, v) \\ C_v(u, v) &= -H_u(u, v) \end{aligned} \quad .$$

*This relation can be written in a compact form $dH = *dC$ using the Hodge $*$ operator.*

4. *If a minimal patch is bounded by a straight line, then its conjugate patch is bounded by a planar symmetry line and vice versa. This can be seen in the catenoid-helicoid examples, where planar meridians of the catenoid correspond to the straight lines of the helicoid.*
5. *Since at every point the length and the angle between the partial derivatives are identical for the surface and its conjugate (i.e. both surfaces are isometric) we have as a result, that the angles at corresponding boundary vertices of surface and conjugate surface are identical.*

The last two properties are most important for the later conjugate surface method.

Review of the Conjugate Surface Construction

Over the last decade the conjugate surface method has been established as one of the most powerful techniques to construct new minimal surfaces with a proposed shape in mind. One of the major drawbacks of the method is the so-called period problem which often prevents a rigorous existence proof of the examples. In these situation

where theoretical techniques fail up to now, a numerical approach is required to allow experiments.

The major obstacle for a numerical simulation of the conjugate surface method is the fact, that the minimal surfaces are usually unstable. Currently, the conjugation method based on discrete minimal surfaces is the only numerical method to compute the conjugate of a polyhedral minimal surface with satisfactory results.

4.6.1 Discrete Conjugate Minimal Surface

In this section we develop the notion of the conjugate and the associate family of a discrete minimal surface. In [87] the discrete conjugation algorithm is based on the concept of discrete harmonic maps, but the method did not unveil the variational properties of the conjugate surface. In the following we first show the area minimality of the conjugate discrete minimal surface, and second, describe a practical algorithm by reformulating the conjugation method of [87] in terms of the conjugation of harmonic maps using conforming and non-conforming functions derived in Chapter 3.

Currently, the method [87] seems to be the only method to allow the conjugation of a numerically computed discrete minimal surface with reasonable results. The main difficulties are to provide accurate C^1 information, which is required for the conjugation, from numerically obtained minimal surfaces.

The remaining part of this section shows that the conjugate minimal surface is well-defined, and derives some important properties. Most results follow from properties of the conjugate harmonic coordinate functions.

Let us review some properties of the differential of a polyhedral map $F : M_h \rightarrow \mathbb{R}^d$ where either $F \in S_h$ or $F \in S_h^*$. At each point $p \in M_h$ the differential $\nabla_p F : T_p M_h \rightarrow T_{F(p)} F(M_h)$ is given by

$$\nabla_p F(v) = \begin{pmatrix} \langle \nabla_p f_1, v \rangle \\ \dots \\ \langle \nabla_p f_d, v \rangle \end{pmatrix} \quad \forall v \in T_p M_h$$

if $F = (f_1, \dots, f_d)$ are the coordinate functions. A map F is said to be harmonic if all coordinate functions are harmonic with respect to the metric of M_h . Recalling the definition of the Hodge $*$ operator directly leads to the following definition by applying the operator on the component functions. We say that a simplicial surface M_h is in S_h respectively S_h^* if the triangulation is edge continuous respectively edge-midpoint continuous.

Definition 102 Let $F = (f_1, \dots, f_d) : M_h \rightarrow \mathbb{R}^d$ be a simplicial map in S_h or S_h^* . The Hodge star operator is defined by

$$*dF|_p(v) := \begin{pmatrix} *df_{1|p}(v) \\ \dots \\ *df_{d|p}(v) \end{pmatrix} = \begin{pmatrix} \langle J\nabla_p f_1, v \rangle \\ \dots \\ \langle J\nabla_p f_d, v \rangle \end{pmatrix} \quad \forall v \in T_p M_h$$

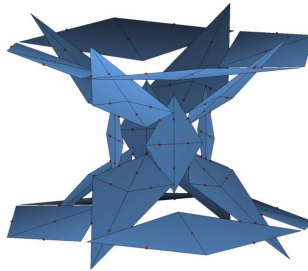
where J is the rotation by $\frac{\pi}{2}$ in the oriented tangent space of each triangle of M_h with respect to the metric in M_h .

For example, if $F = \text{id} : M_h \rightarrow M_h$ is the identity map of a simplicial surface, then we obtain on each triangle

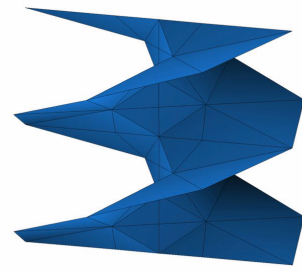
$$*d\text{id}|_p(v) := -Jv \quad \forall v \in T_p M_h. \quad (4.14)$$

Now we are ready to extend the results on discrete harmonic maps of the previous section to the conjugation of simplicial minimal surfaces. In the following theorem we show that the differential $*d\text{id}$ is closed on simplicial minimal surfaces, and that its integral gives the conjugate minimal surface:

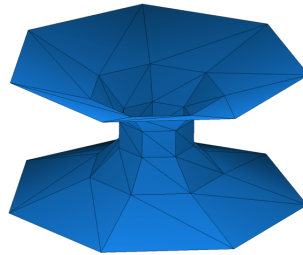
Definition 103 Let M_h be a simplicial minimal surface in S_h (or in S_h^*). Then a discrete conjugate minimal surface M_h^* is a solution of Equation 4.14.



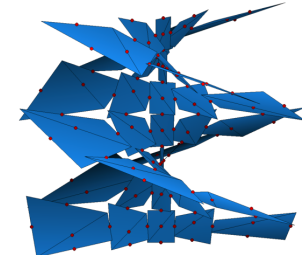
Non-conforming Catenoid.



Conforming Helicoid.



Conforming Catenoid.



Non-conforming Helicoid.

The following theorem justifies this definition and states the general relation between conjugate pairs of discrete minimal surfaces.

Theorem 104 1. Let $M_h \subset \mathbb{R}^d$ be a discrete minimal surface in S_h . Then there exists a conjugate surface $M_h^* \subset \mathbb{R}^d$ in S_h^* which is critical for the area functional in S_h^* .

2. Let $M_h \subset \mathbb{R}^d$ be a discrete minimal surface in S_h^* . Then there exists a conjugate surface $M_h^* \subset \mathbb{R}^d$ in S_h which is critical for the area functional in S_h .

3. M_h^* is uniquely determined by M_h up to translation.

4. M_h and M_h^* are isometric and have the same Gauss map in the sense that corresponding triangles are congruent and parallel.

5. Applying the conjugation twice leads to

$$M_h^{**} = -M_h$$

for a suitably chosen origin.

Proof. Since M_h is a critical for the area functional the identity map

$$\text{id} : M_h \rightarrow M_h$$

is a discrete harmonic map by Corollary 96. Therefore, Theorem 72 in Chapter 3 proves that there exist conjugate harmonic component functions which give rise to a map on M_h

$$\text{id}^* : M_h \rightarrow \mathbb{R}^d.$$

with $M_h^* := \text{id}^* M_h$.

It remains to show that M_h^* is a discrete minimal surface. Here we assume that M_h is in S_h - the case M_h in S_h^* would work with the same words.

We show that M_h^* fulfills the balancing condition. Let $p^* \in M_h^*$ be an interior vertex, then by harmonicity of $\text{id}^* \in S_h^*$ we have

$$\begin{aligned} \frac{d}{dm^*} E_D(\text{id}^*) &= 2(\cot \alpha_{-2}(m^* - m_{-1}^*) + \cot \alpha_{-1}(m^* - m_1^*)) \\ &\quad + \cot \alpha_1(m^* - m_2^*) + \cot \alpha_2(m^* - m_1^*) \\ &= 0 \end{aligned}$$

where m^* and m_i^* are the images of id^* of edge midpoints in M_h .

Since on each triangle id^* is a rotation by $\frac{\pi}{2}$, corresponding triangles of M_h and M_h^* are isometric and have the same angles. Therefore, Equation 4.15 also is the criticality condition of the Dirichlet energy

of the identity map of M_h^* which lies in S_h^* . Thus M_h^* is a discrete minimal surface in S_h^* .

The uniqueness follows from the uniqueness of the conjugate harmonic map and its integration constants. \square

Summarizing, the theorem shows that a conjugate pair of discrete minimal surfaces does not exist in the space of piecewise linear conforming elements S_h but naturally leads to the space of piecewise linear non-conforming Crouzeix-Raviart elements S_h^* . S_h alone is too rigid to contain the conjugate of a minimal surface too.

In other words, if M_h is a simplicial minimal surface in S_h respectively in S_h^* then its discrete conjugate minimal surface M_h^* is the image of the conjugate harmonic $\text{id}^* : M_h \rightarrow \mathbb{R}^d$ map of the identity map of $\text{id} : M_h \rightarrow M_h$, that is, id and id^* fulfill

$$d \text{id}^* = *d \text{id}.$$

The usage of the same domain M_h for both identity maps seems to distinguish M_h from M_h^* but only the conformal structure of the domain surface is relevant for the minimality condition. Therefore, we may instead use M_h^* or, more appropriate, use $\text{id} : M_h \rightarrow M_h$ and $\text{id}^* : M_h^* \rightarrow M_h^*$.

4.6.2 Numerical Conjugation

In practical applications the conjugation of a simplicial minimal surface by rotating each triangle and reassembling the rotated copies requires that the simplicial minimal surface has been computed very exact. Often, minimal surfaces are computed by solving a variational problem where the numerical method stops before reaching the absolute zero of the gradient. A much more stable procedure has been suggested in [87] to circumvent this difficulty: in a minimization procedure based on the Dirichlet energy there exists an accurately computed harmonic map F_i between the last two compute surfaces M_i and M_{i-1} . Instead of by applying the conjugation to the approximation M_i of the limit minimal surface, it is more stable to compute the harmonic conjugate map

$$F_i^* : M_{i-1} \rightarrow M_i^*.$$

The following algorithm summarizes the procedure:

Algorithm 105 *To compute the conjugate M_h^* of the Plateau problem M_h with Dirichlet boundary condition Γ :*

1. Follow the minimization algorithm above to compute a sequence of discrete harmonic maps $F_i : M_i \rightarrow M_{i+1}$.
2. Compute the harmonic conjugate F_i^* of $F_i : M_i \rightarrow M_{i+1}$.
3. Set $M_h := M_{i+1}$ as numerical approximation of the Plateau solution, and set $M_h^* := F_i^*(M_i)$ as approximation of the conjugate minimal surface.

This algorithm generates a sequence of discrete surfaces $\{M_i\}$ and vector-valued harmonic maps $\{F_i : M_i \rightarrow M_{i+1}\}$ which converges to a minimal surface if no degeneration occurs. In order to extend the conjugation technique of the previous sections to the computation of the conjugate of a minimal surface we allow the surfaces M_i to be either all conforming or all non-conforming triangulations. In this case the coordinate functions of each F_i are discrete harmonic functions either in S_h or S_h^* , and the image $F_i^*(M_i)$ of the conjugate harmonic of F_i is a good approximation of the conjugate minimal surface. The two approximations M_h and M_h^* are either a conforming and a non-conforming triangulation, or vice-versa.

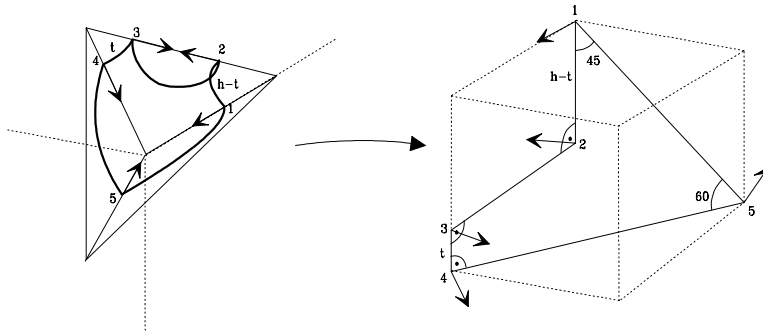


FIGURE 4.3. Transformation of a free-boundary value problem into a family of Dirichlet boundary value problems with a fixed contour.

4.7 Discrete Minimal Catenoid

Examples are important building blocks in the development of a mathematical theory. The first smooth minimal surfaces were found already in the 18th century when Lagrange formulated the variational

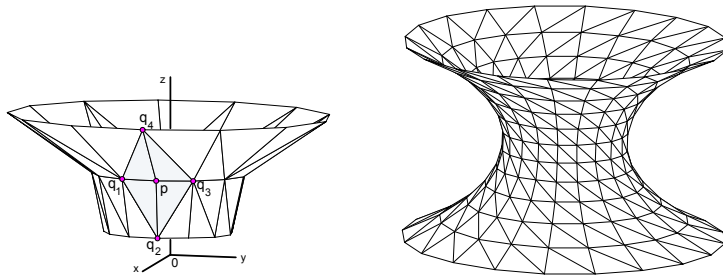


FIGURE 4.4. Discrete catenoid with essential stencil, see Lemma 106

characterization of minimal surfaces. The French geometer and engineer Jean Baptiste Meusnier (1754-1793) recognized the first non-trivial examples of minimal surfaces: the catenoid found by Euler in 1744, also called the chain surface, because it is the surface swept out when one rotates the catenary curve that corresponds to a freely hanging chain about a suitable horizontal line, and the helicoid, or screw surface. Already the discovery of the next examples in 1835 was regarded as so sensational that its discoverer Heinrich Ferdinand Scherk (1798-1885), Professor at Kiel and Bremen, won a prize at the Jablonowski Society at Leipzig in 1831.

The discovery of this discrete minimal catenoid by Polthier and Rossman [94] was driven by a very practical need, namely the provision of an unstable discrete minimal surface for investigations on the index of minimal surfaces. The numerical eigenvalue computations require a very accurate unstable surface as input which is hardly produced by means of minimization methods. Here the explicit formulae allows us to create unstable catenoids of arbitrary resolution. The model [93] at the EG-Models journal includes an interactive applet to study the whole family of discrete catenoids.

The strategy for the construction of an explicit formula for embedded complete discrete minimal catenoids is to assume that the vertices lie on congruent planar polygonal meridians and that the meridians are placed so that the traces of the surfaces will have dihedral symmetry. Under these assumptions we find that the vertices of a discrete meridian lie equally spaced on a smooth hyperbolic cosine curve. Furthermore, these discrete catenoids will converge uniformly in compact regions to the smooth catenoid as the mesh is made finer.

We begin with a lemma that prepares the construction of the vertical meridian of the discrete minimal catenoid, by successively adding one horizontal ring after another starting from an initial ring. Since our construction will lead to pairwise coplanar triangles, the star of each

individual vertex can be made to consist of four triangles (see Remark 147). We now derive an explicit representation of the position of a vertex surrounded by four such triangles in terms of the other four vertex positions. The center vertex is assumed to be coplanar with each of the two pairs of two opposite vertices, with those two planes becoming the plane of the vertical meridian and the horizontal plane containing a dihedrally symmetric polygonal ring (consisting of edges of the surface). See Figure 4.4.

Lemma 106 *Let a, b, d, e be given real numbers with $b \neq e$ and let θ be a dihedral angle which determine four vertices $p = (d, 0, e)$, $q_1 = (d \cos \theta, -d \sin \theta, e)$, $q_2 = (a, 0, b)$, and $q_3 = (d \cos \theta, d \sin \theta, e)$. Then there exists a choice of other real numbers x and y and a fifth vertex $q_4 = (x, 0, y)$ so that the discrete surface formed by the four triangles (p, q_1, q_2) , (p, q_2, q_3) , (p, q_3, q_4) , and (p, q_4, q_1) is minimal, i.e.*

$$\nabla_p \text{area}(\text{star } p) = 0,$$

if and only if

$$2ad > \frac{(e-b)^2}{1+\cos\theta}.$$

Furthermore, x and y are unique and of the form

$$\begin{aligned} x &= \frac{2(1+\cos\theta)d^3 + (a+2d)(e-b)^2}{2ad(1+\cos\theta) - (e-b)^2}, \\ y &= 2e - b. \end{aligned}$$

Proof. First we note that the assumption $b \neq e$ is necessary. If $b = e$, then one may choose $y = b$, and then there is a free 1-parameter family of choices of x , leading to a trivial planar surface.

For simplicity we apply a vertical translation and a homothety about the origin of \mathbb{R}^3 to normalize $d = 1$, $e = 0$, and by doing a reflection if necessary, we may assume $b < 0$. Let $c = \cos \theta$ and $s = \sin \theta$.

We derive conditions for the coordinate components of $\nabla_p \text{area}$ to vanish. The second component vanishes by symmetry of star p . Using the definitions

$$c_1 := \frac{(a-1)s^2 - b^2(1-c)}{\sqrt{2b^2(1-c) + (a-1)^2s^2}}, \quad c_2 := \frac{ab+b}{\sqrt{2b^2(1-c) + (a-1)^2s^2}},$$

the first (resp. third) component of $\nabla_p \text{area}$ vanishes if

$$c_1 = \frac{y^2(1-c) - (x-1)s^2}{\sqrt{2y^2(1-c) + (x-1)^2s^2}}, \quad \text{resp.} \quad c_2 = \frac{-(x-1)y - 2y}{\sqrt{2y^2(1-c) + (x-1)^2s^2}}. \quad (4.16)$$

Dividing one of these equations by the other we obtain

$$x - 1 = \frac{c_2 y(1 - c) + 2c_1}{c_2 s^2 - c_1 y} y, \quad (4.17)$$

so x is determined by y . It now remains to determine if one can find y so that $c_2 s^2 - c_1 y \neq 0$. If $x - 1$ is chosen as in Equation 4.17, then the first minimality condition of Equation 4.16 holds if and only if the second one holds as well. So we only need to insert this value for $x - 1$ into the first minimality condition and check for solutions y . When $c_1 \neq 0$, we find that the condition becomes

$$1 = \frac{c_2 s^2 - c_1 y}{|c_2 s^2 - c_1 y|} \frac{y}{|y|} \frac{-(1 - c)y^2 - 2s^2}{\sqrt{2(1 - c)c_2^2 s^4 + 4c_1^2 s^2 + (2(1 - c)c_1^2 + s^2(1 - c)^2 c_2^2)y^2}}.$$

Since $-(1 - c)y^2 - 2s^2 < 0$, note that this equation can hold only if $c_2 s^2 - c_1 y$ and y have opposite signs, so the equation becomes

$$1 = \frac{(1 - c)y^2 + 2s^2}{\sqrt{2(1 - c)c_2^2 s^4 + 4c_1^2 s^2 + (2(1 - c)c_1^2 + s^2(1 - c)^2 c_2^2)y^2}},$$

which simplifies to

$$1 = \frac{\sqrt{(1 - c)y^2 + 2s^2}}{\sqrt{(1 - c)c_2^2 s^2 + 2c_1^2}}.$$

This implies y^2 is uniquely determined. Inserting the value

$$y = \pm b,$$

one finds that the above equation holds. When $y = b < 0$, we find that $c_2 s^2 - c_1 y < 0$, which is impossible. When $y = -b > 0$, we find that $c_2 s^2 - c_1 y < 0$ if and only if $2a(1 + c) > b^2$. And when $y = -b$ and $2a(1 + c) > b^2$, we have the minimality condition when

$$x = \frac{2 + 2c + ab^2 + 2b^2}{2a + 2ac - b^2}.$$

Inverting the transformation we did at the beginning of this proof brings us back to the general case where d and e are not necessarily 1 and 0, and the equations for x and y become as stated in the lemma. When $c_1 = 0$, we have $(a - 1)(1 + c) = b^2$ and $(x - 1)(1 + c) = y^2$, so, in particular, we have $a > 1$ and therefore $2a(1 + c) > b^2$. The right-hand

side of Equation (4.16) implies $y = -b$ and $x = a$. Again, inverting the transformation from the beginning of this proof, we have that x and y must be of the form in the lemma for the case $c_1 = 0$ as well. \square

The next lemma provides a necessary and sufficient condition for when two points lie on a scaled cosh curve, a condition that is identical to that of the previous lemma. That these conditions are the same is crucial to the proof of the upcoming theorem.

Lemma 107 *Given two points (a, b) and (d, e) in \mathbb{R}^2 with $b \neq e$, and an angle θ with $|\theta| < \pi$, there exists an r so that these two points lie on some vertical translate of the modified cosh curve*

$$\gamma(t) = \left(r \cosh \left[\frac{t}{e-b} \operatorname{arccosh} \left(1 + \frac{1}{r^2} \frac{(e-b)^2}{1+\cos\theta} \right) \right], t \right), \quad t \in \mathbb{R},$$

if and only if $2ad > \frac{(e-b)^2}{1+\cos\theta}$.

Proof. Define $\hat{\delta} = \frac{e-b}{\sqrt{1+\cos\theta}}$. Without loss of generality, we may assume $0 < a \leq d$ and $e > 0$, and hence $-e \leq b < e$. If the points (a, b) and (d, e) both lie on the curve $\gamma(t)$, then

$$\operatorname{arccosh} \left(1 + \frac{\hat{\delta}^2}{r^2} \right) = \operatorname{arccosh} \left(\frac{d}{r} \right) - \operatorname{sign}(b) \cdot \operatorname{arccosh} \left(\frac{a}{r} \right),$$

where $\operatorname{sign}(b) = 1$ if $b \geq 0$ and $\operatorname{sign}(b) = -1$ if $b < 0$. Note that if $b = 0$, then a must equal r (and so $\frac{a}{r} = 1$). This equation is solvable (for either value of $\operatorname{sign}(b)$) if and only if

$$\left(\frac{d}{r} + \sqrt{\frac{d^2}{r^2} - 1} \right) \left(\frac{a}{r} + \sqrt{\frac{a^2}{r^2} - 1} \right) = 1 + \frac{\hat{\delta}^2}{r^2} + \frac{\hat{\delta}}{r} \sqrt{2 + \frac{\hat{\delta}^2}{r^2}}$$

when $b \leq 0$, or

$$\frac{\frac{d}{r} + \sqrt{\frac{d^2}{r^2} - 1}}{\frac{a}{r} + \sqrt{\frac{a^2}{r^2} - 1}} = 1 + \frac{\hat{\delta}^2}{r^2} + \frac{\hat{\delta}}{r} \sqrt{2 + \frac{\hat{\delta}^2}{r^2}}$$

when $b \geq 0$, for some $r \in (0, a]$. The right-hand side of these two equations has the following properties:

1. It is a nonincreasing function of $r \in (0, a]$.

2. It attains some finite positive value at $r = a$.
3. It is greater than the function $2\hat{\delta}^2/r^2$.
4. It approaches $2\hat{\delta}^2/r^2$ asymptotically as $r \rightarrow 0$.

The left-hand sides of these two equations have the following properties:

1. They attain the same finite positive value at $r = a$.
2. The first one is a nonincreasing function of $r \in (0, a]$.
3. The second one is a nondecreasing function of $r \in (0, a]$.
4. The second one attains the value $\frac{d}{a}$ at $r = 0$.
5. The first one is less than the function $4ad/r^2$.
6. The first one approaches $4ad/r^2$ asymptotically as $r \rightarrow 0$.

It follows from these properties that one of the two equations above has a solution for some r if and only if $2ad > \hat{\delta}^2$. This completes the proof. \square

We now derive an explicit formula for discrete minimal catenoids, by specifying the vertices along a planar polygonal meridian. Then the traces of the surfaces will have dihedral symmetry of order $k \geq 3$. The surfaces are tessellated by planar isosceles trapezoids like a \mathbb{Z}^2 grid, and each trapezoid can be triangulated into two triangles by choosing a diagonal of the trapezoid as the interior edge. Either diagonal can be chosen, as this does not affect the minimality of the catenoid, by Remark 147.

The discrete catenoid has two surprising features. First, the vertices of a meridian lie on a scaled smooth cosh curve (just as the profile curve of smooth catenoids lies on the cosh curve), and there is no apriori reason to have expected this. Secondly, the vertical spacing of the vertices along the meridians is constant.

Theorem 108 *There exists a four-parameter family of embedded and complete discrete minimal catenoids $C = C(\theta, \delta, r, z_0)$ with dihedral rotational symmetry and planar meridians. If we assume that the dihedral symmetry axis is the z -axis and that a meridian lies in the xz -plane, then, up to vertical translation, the catenoid is completely described by the following properties:*

1. The dihedral angle is $\theta = \frac{2\pi}{k}$, $k \in \mathbb{N}$, $k \geq 3$.
2. The vertices of the meridian in the xz -plane interpolate the smooth cosh curve

$$x(z) = r \cosh\left(\frac{1}{r}az\right),$$

with

$$a = \frac{r}{\delta} \operatorname{arccosh}\left(1 + \frac{1}{r^2} \frac{\delta^2}{1 + \cos\theta}\right),$$

where the parameter $r > 0$ is the waist radius of the interpolated cosh curve, and $\delta > 0$ is the constant vertical distance between adjacent vertices of the meridian.

3. For any given arbitrary initial value $z_0 \in \mathbb{R}$, the profile curve has vertices of the form $(x_j, 0, z_j)$ with

$$\begin{aligned} z_j &= z_0 + j\delta \\ x_j &= x(z_j) \end{aligned}$$

where $x(z)$ is the meridian in item 2 above.

4. The planar trapezoids of the catenoid may be triangulated independently of each other (by Remark 147).

Proof. By Lemma 106, if we have three consecutive vertices (x_{n-1}, z_{n-1}) , (x_n, z_n) , and (x_{n+1}, z_{n+1}) along the meridian in the xz -plane which satisfy the recursion formula

$$x_{n+1} = \frac{(x_{n-1} + 2x_n)\hat{\delta}^2 + 2x_n^3}{2x_nx_{n-1} - \hat{\delta}^2}, \quad z_{n+1} = z_n + \delta, \quad (4.18)$$

where $\delta = z_n - z_{n-1}$ and $\hat{\delta} = \delta/\sqrt{1 + \cos\theta}$. As seen in Lemma 106, the vertical distance between (x_{n-1}, z_{n-1}) and (x_n, z_n) is the same as the vertical distance between (x_n, z_n) and (x_{n+1}, z_{n+1}) , so we may consider δ and $\hat{\delta}$ to be constants independent of n .

In order for the surface to exist, Lemma 106 requires that

$$2x_nx_{n-1} > \hat{\delta}^2.$$

This implies that all x_n have the same sign, and we may assume $x_n > 0$ for all n . Therefore the surface is embedded. Also, as the condition $2x_nx_{n-1} > \hat{\delta}^2$ implies

$$2x_{n+1}x_n = \frac{2x_n(x_{n-1} + 2x_n)\hat{\delta}^2 + 4x_n^4}{2x_nx_{n-1} - \hat{\delta}^2} > \frac{2x_nx_{n-1}\hat{\delta}^2}{2x_nx_{n-1} - \hat{\delta}^2} > \hat{\delta}^2,$$

we see, inductively, that x_j is defined for all $j \in \mathbb{Z}$. Hence the surface is complete.

One can easily check that the function $x(z)$ in the theorem also satisfies the recursion formula (4.18), in the sense that if $x_j := x(z_j)$, then these x_j satisfy this recursion formula. It only remains to note that, given two initial points (x_{n-1}, z_{n-1}) and (x_n, z_n) with $z_n > z_{n-1}$, there exists an r so that these two points lie on the curve $x(z)$ with our given δ and θ (up to vertical translation) if and only if $2x_n x_{n-1} > \hat{\delta}^2$, as shown in Lemma 107. \square

Remark 109 *If we consider the symmetric example with normalized waist radius $r = 1$, that is if we choose $(x_1, z_1) = (1, 0)$ and $(x_2, z_2) = (1 + \hat{\delta}^2, \delta)$, then the recursion formula in Equation 4.18 implies that*

$$(x_n, z_n) = \left(1 + \sum_{j=1}^{n-1} 2^{j-1} a_{n-1,j} \hat{\delta}^{2j}, (n-1)\delta\right), \quad \text{for } n \geq 3,$$

where $a_{n-1,j}$ is defined recursively by $a_{n,m} = 0$ if $m < 0$ or $n < 0$ or $m > n$, $a_{0,0} = 1$, $a_{n,0} = 2$ if $n > 0$, and $a_{n,m} = 2a_{n-1,m} - a_{n-2,m} + a_{n-1,m-1}$ if $n \geq m \geq 1$. Thus

$$a_{n,m} = \binom{n+m}{2m} + \binom{n+m-1}{2m}.$$

These $a_{n,m}$ are closely related to the recently solved refined alternating sign matrix conjecture [21].

Corollary 110 *There exists a two-parameter family of discrete catenoids $C_1(\theta, z_0)$ whose vertices interpolate the smooth minimal catenoid with meridian $x = \cosh z$.*

Proof. The waist radius of the scaled cosh curve must be $r = 1$. Further, we must choose the parameter $a = 1$ which is fulfilled if θ and δ are related by $1 + \cos \theta + \delta^2 = (1 + \cos \theta) \cosh \delta$. The offset parameter z_0 may be chosen arbitrarily leading to a vertical shift of the vertices along the smooth catenoid. Note that if $z_0 = 0$, we obtain a discrete catenoid that is symmetric with respect to a horizontal reflection. \square

Corollary 111 *For each fixed r and z_0 , the profile curves of the discrete catenoids $C(\theta, \delta, r, z_0)$ approach the profile curve $x = r \cosh \frac{z}{r}$ of a smooth catenoid uniformly in compact sets of \mathbb{R}^3 as $\delta, \theta \rightarrow 0$.*

Proof. This is a direct consequence of the explicit representation of the meridian. Since

$$\lim_{\delta \rightarrow 0} \frac{1}{\delta} \operatorname{arccosh}\left(1 + \frac{1}{r^2} \frac{\delta^2}{1 + \cos \theta}\right) = \frac{\sqrt{2}}{r\sqrt{1 + \cos \theta}},$$

it follows that the profile curve of the discrete catenoid converges uniformly to the curve

$$x = r \cosh \frac{\sqrt{2}z}{r\sqrt{1 + \cos \theta}}$$

as $\delta \rightarrow 0$. Then, as $\theta \rightarrow 0$ we approach the profile curve $x = r \cosh \frac{z}{r}$.
□

4.8 Discrete Minimal Helicoid

We continue with the derivation of explicit discrete helicoids which are a natural second example of a complete, embedded discrete minimal surface. Here we follow the construction of the surface given in [94]. An interactive data set of the model is available at the EG-Models site at [96].

In the smooth setting, there exists an isometric deformation through conjugate surfaces from the catenoid to the helicoid (see, for example, [86]). So, one might first try to make a similar deformation from the discrete catenoids in Theorem 108 to discrete minimal helicoids. But such a deformation is impossible in the space of edge-continuous triangulations. In fact, in order to make an associate family of discrete minimal surfaces, one must allow non-continuous triangle nets having greater flexibility.

Therefore, we adopt a different approach for finding discrete minimal helicoids. The helicoids will be comprised of planar quadrilaterals, each triangulated by four coplanar triangles, see Figures 4.4 and 4.5. Each quadrilateral is the star of a unique vertex, and none of its four boundary edges are vertical or horizontal, and one pair of opposite vertices in its boundary have the same z -coordinate, and the four boundary edges consist of two pairs of adjacent edges so that within each pair the adjacent edges are of equal length.

First we derive an explicit representation for a particular vertex star to be minimal, as this will help us describe helicoids:

Lemma 112 *Let p be a point with a vertex star consisting of four vertices q_1, q_2, q_3, q_4 and four triangles $\triangle_i = (p, q_i, q_{i+1})$, $i \in \{1, 2, 3, 4\}$*

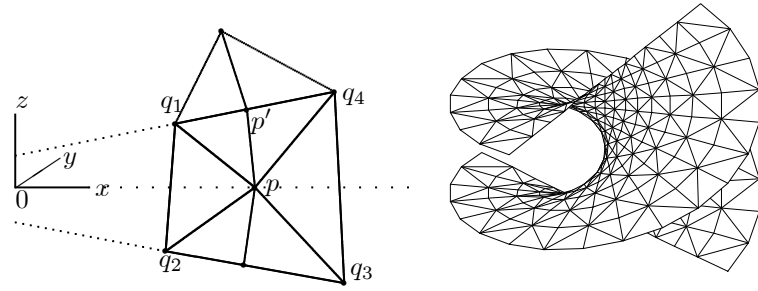


FIGURE 4.5. Essential stencil of the discrete helicoid. $\text{star}(p)$ is the portion considered in Lemma 112, and $\text{star}(p')$ is a planar quadrilateral, like the ones comprising the helicoid in Figure 4.4. Note that the vertex p' can be moved freely inside the planar quadrilateral $\text{star}(p')$ without affecting minimality, by Remark 147. The helicoid on the right uses $x_0 = 0$.

(mod 4). We assume that $p = (u, 0, 0)$, $q_1 = (b \cos \theta, b \sin \theta, 1)$, $q_2 = (b \cos \theta, -b \sin \theta, -1)$, $q_3 = (t \cos \theta, -t \sin \theta, -1)$, $q_4 = (t \cos \theta, t \sin \theta, 1)$ with real numbers $b < u < t$ and $\theta \in (0, \frac{\pi}{2})$. If either

$$t = -b(1 + 2u^2 \sin^2 \theta) + 2u\sqrt{1 + b^2 \sin^2 \theta}\sqrt{1 + u^2 \sin^2 \theta} \quad \text{or}$$

$$b = -t(1 + 2u^2 \sin^2 \theta) + 2u\sqrt{1 + t^2 \sin^2 \theta}\sqrt{1 + u^2 \sin^2 \theta},$$

then ∇_p area vanishes.

Proof. Consider the conormals $J_1 = J(q_2 - q_1)$, $J_2 = J(q_3 - q_2)$, $J_3 = J(q_4 - q_3)$, $J_4 = J(q_1 - q_4)$, where J denotes oriented rotation by angle $\frac{\pi}{2}$ in the triangle Δ_j containing the edge being rotated. Then

$$J_1 = (2\sqrt{1 + b^2 \sin^2 \theta}, 0, 0) \quad \text{and} \quad J_3 = (-2\sqrt{1 + t^2 \sin^2 \theta}, 0, 0).$$

Since

$$\begin{aligned} \langle J_4, (\cos \theta, \sin \theta, 0) \rangle &= 0 \\ \det(J_4, (\cos \theta, \sin \theta, 0), (u - b \cos \theta, -b \sin \theta, -1)) &= 0 \\ |J_4|^2 &= (t - b)^2 \end{aligned}$$

we have that the first component of J_4 (and also of J_2) is

$$\frac{u(t - b) \sin^2 \theta}{\sqrt{1 + u^2 \sin^2 \theta}}.$$

By symmetry, the second and third components of J_2 and J_4 are equal but opposite in sign, hence the second and third components

of $J_1 + J_2 + J_3 + J_4$ are zero. So for the minimality condition to hold at p , we need that the first component of $J_1 + J_2 + J_3 + J_4$ is also zero, that is, we need

$$\frac{u(t-b)\sin^2\theta}{\sqrt{1+u^2\sin^2\theta}} + \sqrt{1+b^2\sin^2\theta} - \sqrt{1+t^2\sin^2\theta} = 0,$$

and the solution of this with respect to b or t is as in the lemma. So, for this solution ∇_p area vanishes. \square

Theorem 113 *There exists a family of complete embedded discrete minimal helicoids, with the connectivity as shown in Figure 4.4. The vertices, indexed by $i, j \in \mathbb{Z}$, are the points*

$$\frac{r \sinh(x_0 + j\delta)}{\sin\theta} (\cos(i\theta), \sin(i\theta), 0) + (0, 0, ir),$$

for any given real numbers $\theta \in (0, \frac{\pi}{2})$ and $r, \delta \in \mathbb{R}$.

Note that these surfaces are invariant under the screw motion that combines vertical upward translation of distance $2r$ with rotation about the x_3 -axis by an angle of 2θ . The term x_0 determines the offset of the vertices from the z -axis (if $x_0 = 0$, then the z -axis is included in the edge set), and δ determines the horizontal spacing of the vertices. The homothety factor is r , which equals the vertical distance between consecutive horizontal lines of edges.

Proof. Without loss of generality, we may assume $r = 1$. So for a given i , the vertices are points on the line $\{s(\cos(i\theta), \sin(i\theta), i) \mid s \in \mathbb{R}\}$, for certain values of s . We choose x_0 and δ so that the $(j-2)$ -th vertex has s -value $s_{j-2} = \sinh(x_0 + (j-2)\delta)/\sin\theta$ and the $(j-1)$ -th vertex has s -value $s_{j-1} = \sinh(x_0 + (j-1)\delta)/\sin\theta$. Lemma 112 implies that the j -th vertex has s -value

$$s_j = -s_{j-2}(1 + 2s_{j-1}^2 \sin^2\theta) + 2s_{j-1} \sqrt{1 + s_{j-2}^2 \sin^2\theta} \sqrt{1 + s_{j-1}^2 \sin^2\theta},$$

a recursion formula that is satisfied by

$$s_j = \sinh(x_0 + j\delta)/\sin\theta.$$

Lemma 112 implies a similar formula for determining s_{j-3} in terms of s_{j-2} and s_{j-1} , with the same solution. Finally, noting that those vertices whose star is a planar quadrilateral can be freely moved inside that planar quadrilateral without disturbing minimality of the surface, the theorem is proved. \square

References

- [1] A. D. Aleksandrov and V. A. Zalgaller. *Intrinsic Geometry of Surfaces*, volume 15 of *Translation of Mathematical Monographs*. AMS, 1967.
- [2] S. B. Alexander and R. L. Bishop. Comparison theorems for curves of bounded geodesic curvature in metric spaces of curvature bounded above. *Diff. Geom. Appl.*, 6(1):67–86, 1996.
- [3] C. Allendoerfer and A. Weil. The Gauss-Bonnet theorem for riemannian polyhedra. *Trans. Amer. Math. Soc.*, 53:101–129, 1943.
- [4] T. Banchoff. Critical points and curvature for embedded polyhedra. *J. Diff. Geom.*, 1:245–256, 1967.
- [5] T. Banchoff. Critical points and curvature for embedded polyhedra ii. *Progress in Math.*, 32:34–55, 1983.
- [6] R. E. Bank and A. H. Sherman. The use of adaptive grid refinement for badly behaved elliptic partial differential equations. *Advances in Computer Methods for Partial Differential Equations*, 3:33–39, 1979.

-
- [7] D. Banks and B. Singer. A predictor-corrector technique for visualizing unsteady flow. *IEEE Transactions on Visualization and Computer Graphics*, 1(2):151–163, June 1995.
- [8] E. Bänsch. Local mesh refinement in 2 and 3 dimensions. *IMPACT of Computing in Science and Engineering*, 3:181–191, 1991.
- [9] J. L. Barbosa and M. d. Carmo. Stability of minimal surfaces and eigenvalues of the laplacian. *Math. Z.*, 173:13–28, 1980.
- [10] H. Battke, D. Stalling, and H.-C. Hege. Fast line integral convolution for arbitrary surfaces in 3d. In H.-C. Hege and K. Polthier, editors, *Visualization and Mathematics*, pages 181–195. Springer Verlag, Heidelberg, 1997.
- [11] B. Baumgart. Winged-edge polyhedron representation. Technical Report STAN-CS-320, Stanford University, 1972.
- [12] E. D. Bloch. *A First Course in Geometric Topology and Differential Geometry*. Birkhäuser Verlag, 1997.
- [13] A. Bobenko and U. Pinkall. Discrete isothermic surfaces. *J. reine angew. Math.*, 475:187–208, 1996.
- [14] A. Bobenko and U. Pinkall. Discretization of surfaces and integrable systems. In A. Bobenko and R. Seiler, editors, *Discrete Integrable Geometry and Physics*. Clarendon Press, Oxford, 1999.
- [15] A. Bossavit. Mixed finite elements and the complex of whitney forms. In J. Whiteman, editor, *The Mathematics of Finite Elements and Applications VI*, pages 137–144. Academic Press, 1988.
- [16] A. Bossavit. *Computational Electromagnetism*. Academic Press, Boston, 1998.
- [17] K. Brakke. *Surface Evolver Manual v2.14*, 1999. <http://www.susqu.edu/facstaff/b/brakke/evolver>.
- [18] K. A. Brakke. The surface evolver. *Exp. Math.*, 1(2):141–165, 1992.
- [19] K. A. Brakke and J. M. Sullivan. Using symmetry features of the surface evolver to study foams. In H.-C. Hege and K. Polthier, editors, *Visualization and Mathematics*, pages 95–117. Springer Verlag, Heidelberg, 1997.

-
- [20] S. C. Brenner and L. R. Scott. *The Mathematical Theory of Finite Element Methods*. Springer Verlag, 1994.
- [21] D. Bressoud and J. Propp. How the alternating sign matrix conjecture was solved. *Notices of the AMS*, 46(6):637–646, 1999.
- [22] N. Burtnyk and M. Wein. Computer generated key-frame animation. *J. Soc. Motion Picture and Television Engineers*, 80:149–153, 1971.
- [23] N. Burtnyk and M. Wein. Interactive skeleton techniques for enhancing motion dynamics in key frame animation. *Communications ACM*, 19(10):564–569, 1976.
- [24] M. P. D. Carmo. *Differential Geometry of Curves and Surfaces*. Prentice-Hall, 1976.
- [25] A. J. Chorin and J. E. Marsden. *A Mathematical Introduction to Fluid Mechanics*. Springer Verlag, 1998.
- [26] P. Ciarlet. *The Finite Element Method for Elliptic Problems*. North-Holland, 1978.
- [27] M. de Berg, M. van Kreveld, M. Overmars, and O. Schwarzkopf. *Computational Geometry*. Springer Verlag, 1997.
- [28] W. C. de Leeuw and R. van Liere. Visualization of global flow structures using multiple levels of topology. In E. Gröller, H. Löffelmann, and W. Ribarsky, editors, *Data Visualization '99*, pages 45 – 52. Springer Verlag, 1999.
- [29] L. de Lima and W. Rossman. On the index of constant mean curvature 1 surfaces in hyperbolic space. *Indiana Math. J.*, 47(2):685–723, 1998.
- [30] L. DeFloriani and E. Puppo. Hierarchical triangulation for multiresolution surface description. *ACM Transactions on Graphics*, 14(4):363–411, October 1995.
- [31] U. Dierkes, S. Hildebrandt, A. Küster, and O. Wohlrab. *Minimal Surfaces*, volume 1 of *Grundlehren der Mathematik*. Springer Verlag, 1992.
- [32] E. Dijkstra. A note on two problems in connection with graphs. *Numer. Math.*, 1:269–271, 1959.

-
- [33] J. Dodziuk. Finite-difference approach to the hodge theory of harmonic forms. *Amer. J. of Math.*, 98(1):79–104, 1976.
- [34] J. Dorfmeister, F. Pedit, and H. Wu. Weierstrass type representation of harmonic maps into symmetric spaces. *Com. Anal. Geom.*, 6:633–667, 1998.
- [35] G. Dziuk. An algorithm for evolutionary surfaces. *Numer. Math.*, 58:603–611, 1991.
- [36] G. Dziuk and J. E. Hutchinson. Finite element approximations and the Dirichlet problem for surfaces of prescribed mean curvature. In H.-C. Hege and K. Polthier, editors, *Mathematical Visualization*, pages 73–87. Springer-Verlag, Heidelberg, 1998.
- [37] M. Eck, T. DeRose, T. Duchamp, H. Hoppe, M. Lounsbery, and W. Stuetzle. Multiresolution analysis of arbitrary meshes. *Computer Graphics (SIGGRAPH '95 Proceedings)*, pages 173–182, August 1995.
- [38] B. Eckmann. Harmonische funktionen und randwertaufgaben in einem komplex. *Commentarii Math. Helvetici*, 17:240–245, 1944–45.
- [39] H. Edelsbrunner, D. Kirkpatrick, and R. Seidel. On the shape of a set of points in the plane. *IEEE Transactions on Information Theory*, 29(4):551–559, 1983.
- [40] H. Edelsbrunner and E. P. Mücke. Three dimensional alpha shapes. *ACM Transactions on Graphics*, 13:43–72, 1994.
- [41] G. Farin. *Curves and Surfaces for CAGD*. Academic Press, 1993.
- [42] D. Fischer-Colbrie. On complete minimal surfaces with finite morse index in three manifolds. *Invent. Math.*, 82:121–132, 1985.
- [43] G. Fix and G. Strang. *An analysis of the finite element method*. Prentice-Hall, 1973.
- [44] M. S. Floater. Parametrization and smooth approximation of surface triangulations. *Computer Aided Geometric Design*, 14:231–250, 1997.
- [45] A. Fournier and W. Reeves. A simple model of ocean waves. *ACM Siggraph 86*, pages 75–84, 1986.

- [46] A. Friedrich, K. Polthier, and M. Schmies. Interpolating triangle hierarchies. In D. Ebert, H. Rushmeier, and H. Hagen, editors, *Proceedings Visualization '98*, pages 391–396. IEEE Computer Society Press, October 1998.
- [47] M. Gromov. *Metric structures for Riemannian and non-Riemannian spaces*, volume 152 of *Progress in Mathematics*. Springer-Verlag, 1999.
- [48] K. Große-Brauckmann. New surfaces of constant mean curvature. *Math. Zeit.*, 214:527–565, 1993.
- [49] K. Große-Brauckmann and K. Polthier. Numerical examples of compact surfaces of constant mean curvature. In B. Chow, R. Gulliver, S. Levy, and J. Sullivan, editors, *Elliptic and Parabolic Methods in Geometry*, pages 23–46, Wellesley (MA), 1996. AK Peters.
- [50] K. Große-Brauckmann and K. Polthier. Compact constant mean curvature surfaces with low genus. *Experimental Mathematics*, 6(1):13–32, 1997.
- [51] K. Große-Brauckmann and K. Polthier. Constant mean curvature surfaces derived from Delaunay’s and Wente’s examples. In H.-C. Hege and K. Polthier, editors, *Visualization and Mathematics*, pages 119–134. Springer Verlag, Heidelberg, 1997.
- [52] C. Gunn, A. Ortmann, U. Pinkall, K. Polthier, and U. Schwarz. Oorange - a visualization environment for mathematical experiments. In H.-C. Hege and K. Polthier, editors, *Visualization and Mathematics*, pages 249–265. Springer Verlag, Heidelberg, 1997.
- [53] I. Guskov, K. Vidimce, W. Sweldens, and P. Schröder. Normal meshes. In *Computer Graphics Proceedings (Siggraph '00)*, pages 95–102, 2000.
- [54] M. Heil. Numerical tools for the study of finite gap solutions of integrable systems. Master’s thesis, Technical University of Berlin, Berlin, 1995.
- [55] J. Helman and L. Hesselink. Representation and display of vector field topology in fluid flow data sets. *IEEE Computer*, 22(8):27–36, August 1989.

-
- [56] J. Helman and L. Hesselink. Visualizing vector field topology in fluid flows. *IEEE Computer Graphics & Applications*, 11(3):36–46, 1991.
- [57] H. Helmholtz. Über Integrale der Hydrodynamischen Gleichungen. *J. Reine Angew. Math.*, 55:25–55, 1858.
- [58] T. Hoffmann. Discrete rotational CMC surfaces and the elliptic billiard. In H.-C. Hege and K. Polthier, editors, *Mathematical Visualization*, pages 117–124. Springer-Verlag, Heidelberg, 1998.
- [59] T. Hoffmann. Discrete H-surfaces and discrete holomorphic maps. In A. Bobenko and R. Seiler, editors, *Discrete Integrable Geometry and Physics*. Oxford Press, 1999.
- [60] H. Hoppe. Progressive meshes. *Computer Graphics (SIGGRAPH '96 Proceedings)*, pages 99–108, August 1996.
- [61] H. Hoppe. View-dependent refinement of progressive meshes. In *Computer Graphics (SIGGRAPH '97 Proceedings)*, pages 189–198, August 1997.
- [62] L. Hsu, R. Kusner, and J. Sullivan. Minimizing the squared mean curvature integral for surfaces in space forms. *Experimental Mathematics*, 1(3):191–207, 1992.
- [63] K. Hurdal, P. L. Bowers, K. Stephenson, D. W. L. Summers, K. Rehm, K. Schaper, and D. A. Rottenberg. Quasi-conformally flat mapping the human cerebellum. In C. Taylor and A. Colchester, editors, *Medical Image Computing and Computer-Assisted Intervention - MICCAI'99*, volume 1679 of *Lecture Notes in Computer Science*, pages 279–286. Springer Verlag, 1999.
- [64] J. E. Hutchinson. Computing conformal maps and minimal surfaces. *Proc. Centr. Math. Anal., Canberra*, 26:140–161, 1991.
- [65] H. Karcher. Construction of minimal surfaces. *Surveys in Geometry, University of Tokyo*, pages 1–96, 1989.
- [66] H. Karcher. The triply periodic minimal surfaces of A. Schoen and their constant mean curvature companions. *Man. Math.*, 64:291–357, 1989.

- [67] H. Karcher and K. Polthier. Construction of triply periodic minimal surfaces. In J. Klinowski and A. L. Mackay, editors, *Curved Surfaces in Chemical Structures*, volume 354 (1715) of *A*, pages 2077–2104. The Royal Society, London, Great Britain, phil. trans. r. soc. lond. edition, September 1996.
- [68] Z. Karni and C. Gotsman. Spectral compression of mesh geometry. In *Computer Graphics Proceedings (Siggraph '00)*, pages 279–286. ACM SIGGRAPH, 2000.
- [69] M. Kilian, I. McIntosh, and N. Schmitt. New constant mean curvature surfaces. *Exp. Math.*, 9(4):595–611, 2000.
- [70] C. L. Lawson. Transforming triangulations. *Discrete Math.*, 3:365–372, 1972.
- [71] C. L. Lawson. Software for C^1 surface interpolation. In J. R. Rice, editor, *Math. Software III*, pages 161–194. Academic Press, 1977.
- [72] H. B. Lawson. *Lectures on Minimal Submanifolds*. Publish or Perish Press, 1971.
- [73] H. B. Lawson. Complete minimal surfaces in S^3 . *Ann. of Math.*, 92:335–374, 1992.
- [74] H. Lee, L. Kim, M. Meyer, and M. Desbrun. Meshes on fire. In N. Magnenat-Thalmann and D. Thalmann, editors, *Computer Animation and Simulation 2001*, Computer Science. Springer Verlag, 2001. Proceedings of the Eurographics Workshop.
- [75] N. Magnenat-Thalmann and D. Thalmann. *Computer Animation*. Computer Science Workbench. Springer Verlag, second edition, 1985.
- [76] N. Max. Carla’s island. ACM Siggraph 81 Video Review, 1981. Animation.
- [77] J. S. B. Mitchell, D. M. Mount, and C. H. Papadimitriou. The discrete geodesic problem. *SIAM J. Comput.*, 16(4):647–668, 1987.
- [78] E. E. Moise. *Geometric Topology in Dimensions 2 and 3*. Springer Verlag, New York, 1977.

- [79] S. Montiel and A. Ros. Schrödinger operators associated to a holomorphic map. In *Global Differential Geometry and Global Analysis*, volume 1481 of *Lect. Notes in Math.*, pages 147–174. Springer Verlag, 1991.
- [80] S. Müller, M. Struwe, and V. Sverak. Harmonic maps on planar lattices. Technical Report 17, MPI Leipzig, 1997.
- [81] J. R. Munkres. *Elements of Algebraic Topology*. Addison Wesley, 1984.
- [82] S. Nayatani. Lower bounds for the Morse index of complete minimal surfaces in Euclidean 3-space. *Osaka J. Math.*, 27:453–464, 1990.
- [83] S. Nayatani. Morse index of complete minimal surfaces. In M. Rassias, editor, *The Problem of Plateau*, pages 181–189. World Scientific, 1992.
- [84] S. Nayatani. Morse index and gauß maps of complete minimal surfaces in Euclidean 3-space. *Comment. Math. Helv.*, 68:511–537, 1993.
- [85] B. Oberknapp and K. Polthier. An algorithm for discrete constant mean curvature surfaces. In H.-C. Hege and K. Polthier, editors, *Visualization and Mathematics*, pages 141–161. Springer Verlag, Heidelberg, 1997.
- [86] R. Osserman. *A Survey of Minimal Surfaces*. Dover, 1986.
- [87] U. Pinkall and K. Polthier. Computing discrete minimal surfaces and their conjugates. *Experim. Math.*, 2(1):15–36, 1993.
- [88] A. V. Pogorelov. Quasigeodesic lines on a convex surface. *Amer. Math. Soc. Transl.*, I. Ser. 6(72):430–473, 1952.
- [89] E. Polak. *Computational Methods in Optimization*. Academic Press, 1971.
- [90] K. Polthier. Geometric a priori estimates for hyperbolic minimal surfaces. *Bonner Mathematische Schriften*, 263, 1994.
- [91] K. Polthier. JavaView homepage, 1998–2002. <http://www.javaview.de/>.

- [92] K. Polthier, S. Khadem-Al-Charieh, E. Preuß, and U. Reitebuch. Publication of interactive visualizations with JavaView. In J. Borwein, M. H. Morales, K. Polthier, and J. F. Rodrigues, editors, *Multimedia Tools for Communicating Mathematics*. Springer Verlag, 2002. <http://www.javaview.de>.
- [93] K. Polthier and W. Rossman. Discrete catenoid. *Electronic Geometry Models*, 2000. <http://www.eg-models.de/2000.05.002/>.
- [94] K. Polthier and W. Rossman. Discrete constant mean curvature surfaces and their index. Report 484, SFB 288, TU-Berlin, 2000. To appear in: *J. Reine Angew. Math.*
- [95] K. Polthier and W. Rossman. Counterexample to the maximum principle for discrete minimal surfaces. *Electronic Geometry Models*, 2001. <http://www.eg-models.de/2000.11.040/>.
- [96] K. Polthier and W. Rossman. Discrete minimal helicoid. *Electronic Geometry Models*, 2001. <http://www.eg-models.de/2001.01.046/>.
- [97] K. Polthier and W. Rossman. Discrete constant mean curvature surfaces and their index. *J. reine angew. Math*, 549(47–77), 2002.
- [98] K. Polthier and M. Rumpf. A concept for time-dependent processes. In M. Göbel, H. Müller, and B. Urban, editors, *Visualization in Scientific Computing*, pages 137–153. Springer Verlag, 1995.
- [99] K. Polthier and M. Schmies. Straightest geodesics on polyhedral surfaces. In H.-C. Hege and K. Polthier, editors, *Mathematical Visualization*, pages 135–150. Springer Verlag, Heidelberg, 1998.
- [100] K. Polthier and M. Schmies. Geodesic flow on polyhedral surfaces. In E. Gröller and H. Löffelmann, editors, *Data Visualization*. Springer Verlag, 1999.
- [101] K. Polthier, M. Schmies, M. Steffens, and C. Teitzel. Geodesics and waves. Siggraph'97 Video Review 120 and VideoMath Festival at ICM'98, 1997. Video, 4:40 min.
- [102] W. H. Press, S. A. Teukolsky, W. T. Vetterling, and B. P. Flannery. *Numerical Recipes in C: The Art of Scientific Computing*. Cambridge University Press, 1993. <http://www.nr.com/>.

-
- [103] Y. G. Reshetnyak. *Geometry IV*, volume 70 of *Encyclopaedia of Mathematical Sciences*, chapter 1. Two-Dimensional Manifolds of Bounded Curvature, pages 3–164. Springer Verlag, 1993.
- [104] W. C. Rheinboldt and C. K. Mesztenyi. On a data structure for adaptive finite element mesh refinements. *ACM Transactions on Mathematical Software*, 6:166–187, 1980.
- [105] M. Rivara. Algorithms for refining triangular grids suitable for adaptive and multigrid techniques. *International J. for Numerical Methods in Engineering*, 20:745–756, 1984.
- [106] M. Roth and R. Peikert. A higher-order method for finding vortex core lines. In D. Ebert, H. Hagen, and H. Rushmeier, editors, *Proc. Visualization '98*, pages 143 – 150. IEEE Computer Society Press, 1998.
- [107] M. Rudin. An unshallow triangulation of a tetrahedron. *Bull. Amer. Math. Soc.*, 64:90–91, 1958.
- [108] I. A. Sadarjoen and F. H. Post. Geometric methods for vortex extraction. In E. Gröller, H. Löffelmann, and W. Ribarsky, editors, *Data Visualization '99*, pages 53 – 62. Springer Verlag, 1999.
- [109] I. A. Sadarjoen, F. H. Post, B. Ma, D. Banks, and H. Pagen-darm. Selective visualization of vortices in hydrodynamic flows. In D. Ebert, H. Hagen, and H. Rushmeier, editors, *Proc. Visualization '98*, pages 419 – 423. IEEE Computer Society Press, 1998.
- [110] G. Scheuermann, H. Hagen, and H. Krüger. Clifford algebra in vector field visualization. In H.-C. Hege and K. Polthier, editors, *Mathematical Visualization*, pages 343–351. Springer-Verlag, Heidelberg, 1998.
- [111] G. Scheuermann, H. Hagen, H. Krüger, M. Menzel, and A. Rockwood. Visualization of higher order singularities in vector fields. In R. Yagel and H. Hagen, editors, *Proc. Visualization '97*, pages 67–74. IEEE Computer Society, 1997.
- [112] Sfb256. *GRAPE Manual*. Sonderforschungsbereich 256, University of Bonn, Sept. 1995. <http://www-sfb256.iam.uni-bonn.de/grape/main.html>.
- [113] M. Sharir and A. Schorr. On shortest paths in polyhedral space. *SIAM J. Comput.*, 15(1):193–215, 1986.

-
- [114] S. N. Steketee and N. I. Badler. Parametric keyframe interpolation incorporating kinetic adjustment and phrasing control. *Computer Graphics (SIGGRAPH '85 Proceedings)*, pages 255–262, 1985.
 - [115] G. Taubin and J. Rossignac. Geometric compression through topological surgery. *ACM Transactions on Graphics*, 17(2):84–115, 1998.
 - [116] M. Tittgemeyer, G. Wollny, and F. Kruggel. Visualising deformation fields computed by non-linear image registration. *Computing and Visualization in Science*, 2002. to appear.
 - [117] T. Tsuchiya. Discrete solutions of the Plateau problem and its convergence. *Math. of Comp.*, 49:157–165, 1987.
 - [118] D. F. Watson. Computing the n-dimensional delaunay tessellation with application to voronoi polytopes. *Comp. J.*, 24:167–172, 1981.
 - [119] H. Whitney. *Geometric Integration Theory*. Princeton University Press, 1957.
 - [120] G. M. Ziegler. *Lectures on Polytopes*. Springer Verlag, 1998. 2nd ed.